Water Resources Research

RESEARCH ARTICLE
10.1029/2022WR033934

Strange Storms: Rainfall Extremes From the Remnants of Hurricane Ida (2021) in the Northeastern US

James A. Smith[1], Mary Lynn Baeck[1], Yibing Su[1], Maofeng Liu[2], and Gabriel A. Vecchi[3]

[1]Civil & Environmental Engineering, Princeton University, Princeton, NJ, USA, [2]Rosenstiel School of Marine and Atmospheric Sciences, University of Miami, Miami, FL, USA, [3]Department of Geosciences, Princeton University, Princeton, NJ, USA

Key Points:

- Remnants of Hurricane Ida produced unprecedented short-duration rainfall extremes at 1–3 hr time scale
- Supercells were the principal agents of extreme rainfall and flooding
- Extratropical Transition of Ida contributed to the environment of record short-duration rainfall

Correspondence to:

J. A. Smith,
jsmith@princeton.edu

Citation:

Smith, J. A., Baeck, M. L., Su, Y., Liu, M., & Vecchi, G. A. (2023). Strange storms: Rainfall extremes from the remnants of Hurricane Ida (2021) in the northeastern US. *Water Resources Research*, *59*, e2022WR033934. https://doi.org/10.1029/2022WR033934

Received 20 OCT 2022
Accepted 5 MAR 2023

Abstract On 1 September 2021, the remnants of Hurricane Ida transformed into a lethal variant of tropical cyclone in which unprecedented short-duration rainfall from clusters of supercells produced catastrophic flooding in watersheds of the Northeastern US. Short-duration rainfall extremes from Ida are examined through analyses of polarimetric radar fields and rain gauge observations. Rainfall estimates are constructed from a polarimetric rainfall algorithm that is grounded in specific differential phase shift (K_{DP}) fields. Rainfall accumulations at multiple locations exceed 1000-year values for 1–3 hr time scales. Radar observations show that supercells are the principal agents of rainfall extremes. Record flood peaks occurred throughout the eastern Pennsylvania—New Jersey region; the peak discharge of the Elizabeth River is one of the most extreme in the eastern US, based on the ratio of the peak discharge to the sample 10-year flood at the gaging station. As with other tropical cyclones that have produced record flooding in the Northeastern US, Extratropical Transition was a key element of extreme rainfall and flooding from Ida. Tropical and extratropical elements of the storm system contributed to extremes of atmospheric water balance variables and Convective Available Potential Energy, providing the environment for extreme short-duration rainfall from supercells.

1. Introduction

On 1 September 2021, the remnants of Hurricane Ida produced unprecedented rainfall and catastrophic flooding in watersheds of the Mid-Atlantic and Northeastern US, with more than 50 flood fatalities (Beven et al., 2022; Figure 1). At numerous locations, 1–3 hr rainfall accumulations were markedly larger than 1000-year values from NOAA Atlas 14 (Bonin et al., 2016). Supercell thunderstorms were the agents of extreme, short-duration rainfall. Record flood peaks were measured at numerous U. S. Geological Survey (USGS) stream gaging stations on 1 and 2 September. The 2 September 2021 flood peak at the Elizabeth River gaging station, which has a record length of 100 years, was more than 3 times larger than the second largest flood peak, which occurred on 28 August 2011 from Hurricane Irene. The peak discharge was more than 5 times larger than the sample 10-year flood magnitude, making it one of the most extreme flood peaks in the eastern US (Smith et al., 2018).

In this study, we document short-duration rainfall extremes through analyses of polarimetric radar fields and rain gauge observations. Rainfall fields are computed from WSR-88D polarimetric radar measurements using an algorithm based on specific differential phase shift, K_{DP} (Section 2; see Chandrasekar et al., 1990; Chaney et al., 2022; Giangrande & Ryzhkov, 2008; A. V. Ryzhkov et al., 2005). The polarimetric upgrade of the WSR-88D radar network in the US, which began in 2012, has resulted in major advances in rainfall estimation (see A. Ryzhkov et al., 2022 for a summary of polarimetric methods and discussion of potential for future advances; see also Zhang et al., 2016). Specific differential phase shift fields have been generally employed for extreme rainfall environments and specifically for settings in which hail is a component of the hydrometeor population sampled by the radar (Kumjian, 2013; A. Ryzhkov et al., 2022).

A supercell is a thunderstorm characterized by the presence of a mesocyclone—a deep, persistently rotating updraft (Markowski & Richardson, 2011). Supercells have been discounted as heavy rainfall producers based on arguments revolving around low precipitation efficiency and rapid storm motion (for background on this perspective, see the text by Cotton and Anthes (1989)). More generally, the relationships between convective intensity and extreme rain have been the subject of recent research, with supercells representing the extremes of convective intensity (see Zipser & Liu, 2022 for a review). Mounting evidence has pointed to supercells and mesovortices as important agents of extreme short-duration rainfall and flash flooding (e.g., Doswell et al., 1996; Nielsen & Schumacher, 2020a; Nielsen & Schumacher, 2020b; Smith et al., 2001, 2018; Zipser & Liu, 2022). Based on

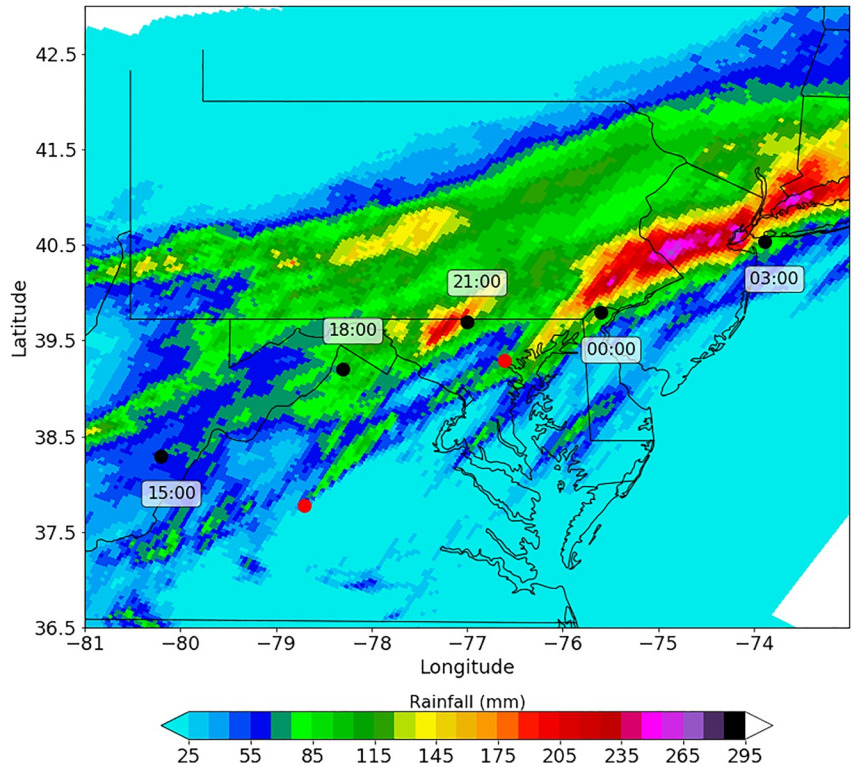

Figure 1. Storm total rainfall (mm) from Stage IV rainfall fields, with locations of Ida (from Storm Prediction Center surface analyses) shown as black circles with time (UTC) on 1 and 2 September. The time period for the storm total is from 00 UTC on 1 to 12 September UTC on 2 September. Red circles show initiation and dissipation locations for long-track supercell in the Mid-Atlantic region (Section 5).

numerical simulations, Nielsen & Schumacher, 2018 conclude that low-level rotation can enhance updrafts and rainfall accumulations (see Markowski & Richardson, 2011; Nielsen & Schumacher, 2020a for additional details).

Rainfall variability in time and space plays an important role in extreme flood response (e.g., Braud et al., 2014; Morin et al., 2006), but a broad theoretical foundation for rainfall variability has proven elusive. In Sections 4 and 5, we present analyses of rainfall variability that characterize key ingredients of short-duration rainfall extremes for the remnants of Hurricane Ida. Lagrangian analyses of the structure, motion and evolution of supercells provide a framework for examining rainfall variability for Ida. These analyses build on previous studies in which high-resolution measurements from radar have been used with storm tracking algorithms to relate Lagrangian properties of storms to rainfall extremes (Dixon & Wiener, 1993; see also Smith et al., 2019).

Polarimetric radar studies have provided major advances in understanding the dynamics and microphysical processes associated with supercells that produce tornadoes (e.g., Kumjian, 2011; Kumjian & Ryzhkov, 2008; Loeffler et al., 2020; Romine et al., 2008; Snyder et al., 2015). Observations of the evolving 3-D structures of polarimetric radar fields have contributed to enhanced understanding of storm kinematics—notably properties of updrafts and downdrafts—and of storm microphysics. These studies provide a foundation for examining polarimetric signatures of extreme rainfall from supercells.

Supercells from Ida produced multiple tornadoes in Maryland, Pennsylvania, and New Jersey on 1 September 2021, including an EF3 tornado in New Jersey and two EF2 tornadoes in eastern Pennsylvania (Beven et al., 2022). Tropical cyclone tornadoes are not unprecedented in the region, but they are rare. Schultz and Cecil (2009) report three tropical cyclone tornadoes in New Jersey during the period from 1950 to 2007 (see also Edwards, 2012). The environment of tropical cyclone supercells has been examined in McCaul (1991) (see also Edwards, 2012). Notable examples of tropical cyclones producing supercells, tornadoes and extreme short-duration rainfall include Hurricanes Harvey (2017; see Edwards et al., 2018; Nowotarski et al., 2021) and Beulah (1967; see Edwards et al., 2018; Smith et al., 2018).

Tropical cyclones are principal agents of extreme floods in the Northeastern US (Villarini & Smith, 2010). Like most tropical cyclones that produce extreme flooding in the region, Extratropical Transition (Atallah & Bosart, 2003; Hart & Evans, 2001; Liu & Smith, 2016) is a central feature of extreme rainfall and flooding from Ida. Tropical and extratropical elements of the storm system contributed to extremes in the atmospheric water balance, as detailed in Section 3. In addition to water balance extremes, Extratropical Transition contributed to the environment for supercell thunderstorms, with large values of Convective Available Potential Energy (CAPE) and wind shear. Storm environment was also tied to key features of supercell organization. Extreme rainfall was associated with both long-lived supercells and clusters of supercells (see Bunkers et al., 2006; Davenport, 2021 for discussion of long-lived supercells and Knupp et al., 2014 for background on clusters of supercells).

The magnitudes of rainfall accumulations in the Northeastern US from Ida exceeded estimates of 1000-year return interval values at 1–3 hr time scales, as detailed in Section 4. Over the past decade, evidence for increasing short-duration rainfall extremes in a warming climate has mounted (Fowler et al., 2021; Prein et al., 2016; Westra et al., 2014; see DeGaetano & Tran, 2021 for analyses of changing rainfall extremes in New Jersey). The availability of radar rainfall data sets covering the past two decades creates an important resource for climatological assessments of rainfall extremes and flood hazards; analyses of rainfall extremes based on radar rainfall data sets will provide increasingly important tools for hydroclimatological analyses (Saltikoff et al., 2019; see also Allen & DeGaetano, 2005; Ghebreyesus & Sharif, 2021; Marra et al., 2017; McGraw et al., 2019; Molter et al., 2021; Overeem et al., 2009; Smith et al., 2012). Accurate estimates of short-duration rainfall extremes are critical for radar-based frequency analysis tools and remain an important area of research (e.g., Lengfeld et al., 2020; Molter et al., 2021; Schleiss et al., 2020; Seo et al., 2014; Wright et al., 2013, 2020).

Rainfall analyses for Ida are also relevant for assessments of Probable Maximum Precipitation (PMP) in the eastern US. Climate change has introduced growing uncertainties in PMP products, which are used to determine design storms for high-hazard structures subject to extreme floods (e.g., Kunkel et al., 2013). Development of storm catalogs of extreme rainfall events is the lynchpin for computing PMP (AWA, 2019; Hansen, 1987; NRC, 1994; Schreiner & Riedel, 1978; World Meteorological Organization, 2009). Estimates of PMP using Storm Transposition are especially sensitive to the accuracy of rainfall estimates for the most extreme events (e.g., World Meteorological Organization, 2009; Wright et al., 2014). Radar rainfall estimates, like those presented in Sections 4 and 5 for Ida, will play an increasingly important role in hydrometeorological analyses of rainfall extremes based on storm catalogs.

Smith et al. (2018) introduced the term "Strange Floods" to characterize record floods that are not just markedly larger than other flood events, but also result from unusual flood agents. The central idea is that flood peak distributions can result from mixtures of different flood agents and the upper tail may be determined by rare events that are poorly represented in observational records. Hirschboeck (1987) introduced the notion that flood regimes can be distinguished by those in which record events result from extremes of common events (see also Marra et al., 2018; Zorzetto et al., 2016) or from unusual events (see also Smith et al., 2011; Villarini & Smith, 2010). Assessing the upper tail of rainfall or flood distributions based on extreme value methods is especially challenging for Strange Floods. As detailed in Sections 4 and 5, tropical cyclone supercells in the Northeastern US are agents of Strange Floods and represent a challenging addition to estimation of short-duration rainfall extremes and flood peaks.

The main results of this study are presented in Sections 3–5. Data and methods are introduced in Section 2, focusing on the rainfall estimation tools that are central to analyses in Sections 3–5. In Section 3, we introduce elements of the storm environment for extreme rainfall on 1–2 September 2021. Documenting rainfall and flood extremes from the remnants of Ida is the principal goal of Section 4. We focus on the region of peak rainfall and flooding in eastern Pennsylvania and New Jersey. The three regions used to organize rainfall and flood analyses in Section 4 (eastern Pennsylvania, central New Jersey, and northern New Jersey) provide the structure in Section 5 for documenting the role of supercells as agents of extreme rainfall. The role of tropical cyclones as extreme flood agents in the Northeastern US provides the organizing theme for Section 6. Conclusions are summarized in Section 7.

2. Data and Methods

Radar rainfall estimates are constructed from WSR-88D (Weather Surveillance Radar—1988 Doppler) polarimetric radar fields derived from the Fort Dix radar in New Jersey (KDIX). We use volume scan Level II polarimetric

fields, which are downloaded from the National Center for Environmental Information (see Data Availability section). The principal polarimetric measurements we use are horizontal reflectivity, Z, and differential phase shift, ϕ_{DP} (in degrees). The specific differential phase shift, K_{DP} (degrees km^{-1}), is the range derivative of ϕ_{DP}; we compute K_{DP} using the Bringi method (with default parameters) implemented in CSU Radar Tools (see Lang et al., 2007; Reimel & Kumjian, 2021 for summaries; see also Wang & Chandrasekar, 2009). Kumjian (2013) and A. Ryzhkov et al. (2022) provide detailed introductions to polarimetric radar measurements, including K_{DP}.

Volume-scan polarimetric radar fields are converted to Cartesian grids with 0.5-km resolution using the Python ARM Radar Toolkit routines (Py-ART; Helmus & Collis, 2016). Rain rate fields are computed from all low elevation scans, which for the KDIX measurements during Ida have an elevation angle of approximately 0.53°. The time resolution of low elevation scans is approximately 2 min. Multiple low-elevation scans within a volume scan were implemented for the WSR-88D system through the SAILS (Supplemental Adaptive Intra-Volume Low-Level Scan) and MESO-SAILS (Multiple Elevation Scan Option for SAILS) scanning strategies (Cho et al., 2022; Kingfield & French, 2022). Although principally targeting tornado and severe weather forecasts (see, e.g., M. S. Van Den Broeke, 2015), the multiple low-elevation scan strategies provide important insights to rainfall variability, especially for watersheds experiencing extreme, short-duration rainfall (Section 5; see also Chaney et al., 2022; Cho et al., 2022). We used manual quality control procedures to check whether incomplete beam filling, ground returns or biological scatterers adversely affected polarimetric fields; no issues were found that affect rainfall analyses.

We focus on K_{DP} estimates of extreme rainfall, with horizontal reflectivity, Z, used for estimating lower rain rates. We follow previous studies (see, e.g., Chandrasekar et al., 1990; Chaney et al., 2022), in using a K_{DP} power law equation when reflectivity is large and K_{DP} noise is modest. Specifically, for reflectivity greater than 45 dBZ and K_{DP} greater than 0.1° km^{-1}, rainfall rate R (in mm h^{-1}) is estimated as:

$$R = a \times {K_{DP}}^{b} \tag{1}$$

For the power law parameters, we take $a = 44.0$ and $b = 0.822$ (A. Ryzhkov et al., 2022). If the two conditions above do not both hold, rainfall rate is estimated using a Z-R relationship:

$$R = \alpha \times Z^{\beta} \tag{2}$$

where Z is in linear units (mm^6 m^{-3}), $\alpha = 0.017$ and $\beta = 0.71$ (see Fulton et al., 1998).

Our focus on K_{DP} for rainfall estimation is based in part on the prevalence of "hail with rain" in the operational NWS Hydrometeor Classification Algorithm (Giangrande & Ryzhkov, 2008; A. Ryzhkov et al., 2022), especially for the areas of heaviest rainfall from Ida. The hail hydrometeor classification is a common feature of supercells. Application of K_{DP} for rainfall estimation has also been recommended for extreme rainfall, dating back to early studies (e.g., Chandrasekar et al., 1990). Our approach to rainfall estimation provides a direct approach for assessing the utility of K_{DP} for estimating extreme rainfall.

Rain gauge observations are used in combination with polarimetric fields for rainfall analyses. Daily observations from the CoCoRaHS (Community Collaborative Rain, Hail, and Snow) network provide the bulk of rain gauge observations. Sub-hourly rain gauge data from the Rutgers New Jersey Weather Network and the USGS also provide key observations for assessing extreme rainfall from Ida. We use daily observations from CoCoRaHS for assessing multiplicative bias of polarimetric rainfall fields computed from Equations 1 and 2. Bias correction of radar rainfall fields based on rain gauge observations has been an important element of rainfall estimation (e.g., Seo et al., 1999; Smith & Krajewski, 1991). Bias correction is used for both operational forecasting (Berne & Krajewski 2013; Imhoff et al., 2021) and for climatological applications (e.g., Smith et al., 2012).

We follow regional bias correction procedures (Smith et al., 2012; Zhou et al., 2019), with mean field bias computed as the ratio of the sum of rainfall from rain gauge observations to the sum of radar rainfall accumulations for locations of rain gages. In Figure 2 (top), we show the regional domain used for bias correction and locations of CoCoRaHS gauges. The domain covers portions of eastern Pennsylvania, central New Jersey, and northern New Jersey. A scatterplot of rainfall observations from gauges and radar are shown in Figure 2 (bottom); radar rainfall estimates are bias-corrected. The multiplicative bias of 1.4 is used throughout our analyses below.

Regional analyses of rainfall over the eastern US are based on the Stage IV radar rainfall fields developed by the National Weather Service (Figure 1). The spatial resolution of these rainfall fields is approximately 4 km and the

10.1029/2022WR033934

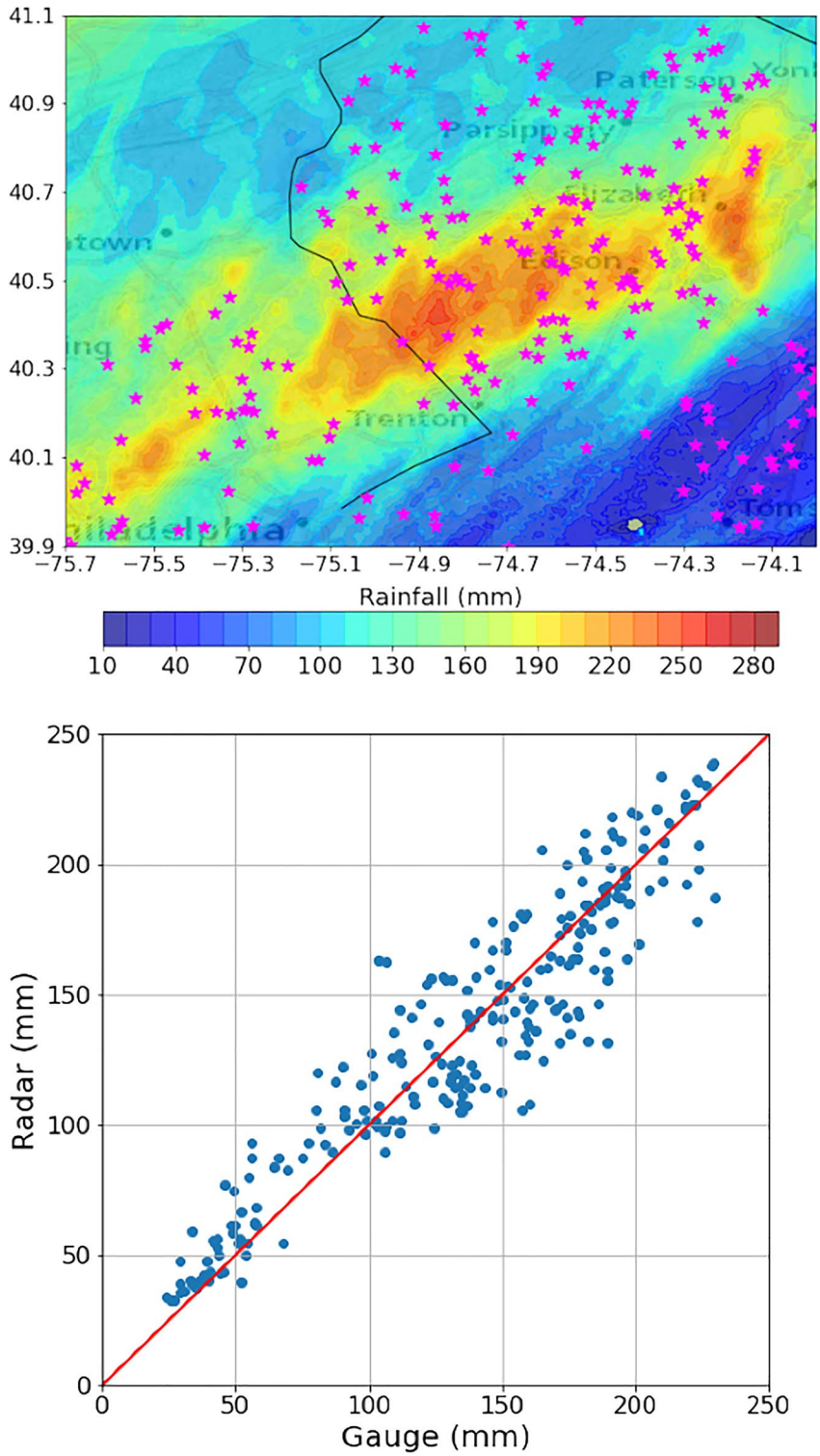

Figure 2. Bias-corrected storm total rainfall (mm) from K_{DP}-based algorithm, with locations of CoCoRaHS rain gauges used for bias correction (top); scatterplot of storm total rain gauge and bias-corrected radar accumulations (bottom). The time period for the bias computation is 12 UTC on 1 to 12 September UTC on 2 September.

time resolution is hourly (Lin & Mitchell, 2005). Stage IV rainfall fields have been increasingly used for climatological applications (e.g., Ghebreyesus & Sharif, 2021).

We identify supercells through local maxima in azimuthal shear fields computed from Doppler velocity measurements using the SPORK-SPIN algorithms (Van Den Broeke, 2021; M. Wilson and Van Den Broeke, 2021; Wilson et al., 2020). We use a threshold of 1.0 m s^{-1} km^{-1} for identifying mesocyclones.

Analyses of storm environment utilize model fields from the Global Data Assimilation System (GDAS; Derber et al., 1991). We compute components of the atmospheric water balance using GDAS fields and procedures described in Su and Smith (2021). We also use GDAS fields for analyses of Extratropical Transition based on cyclone phase space methods (Hart & Evans, 2001).

3. Storm Environment

The remnants of Hurricane Ida passed through the Mid-Atlantic and Northeastern US on 1 September, with the center of circulation moving from southwestern Virginia at local noon past New York City by midnight local time (Figure 1; UTC is local time plus 4 hr). Rainfall accumulations exceeding 200 mm extend in an arc from southeastern Pennsylvania through New Jersey and New York into Connecticut (Figure 1). Rainfall along this arc was concentrated during the 6-hr period beginning at 2000 UTC on 1 September.

Extratropical Transition—in which a warm core, symmetric tropical cyclone transitions to a cold core, asymmetric cyclone (Hart & Evans, 2001)—was a prominent feature of the storm environment on 1 September, as is the case for most major tropical cyclone flood events in the Northeastern US (Atallah & Bosart, 2003; Atallah et al., 2007; Liu & Smith, 2016). Ida completed its transition to a cold core, asymmetric cyclone by 12 UTC on 1 September based on cyclone phase space analyses of GDAS model fields (figure not shown; see Hart & Evans, 2001; Liu et al., 2017 for discussion of methods). At that time, the center of circulation of the storm was located southwest of the domain shown in Figure 1.

As the storm moved up the East Coast on 1 September, extreme rainfall was organized along and south of a warm front. At 12 UTC the warm front extended through Maryland into southern New Jersey (Figure 3). By 00 UTC on 2 September, the frontal boundary was located in northern New Jersey, with a surface low in southeastern Pennsylvania along the New Jersey border.

Tropical and extratropical features of Ida contributed to extremes of the atmospheric water balance (Figure 4). Precipitable water values peaked between 18 UTC on 1 September and 00 UTC on 2 September, with values exceeding 65 mm near in southeastern Pennsylvania near Philadelphia at 0000 UTC, approaching record values for the region. Peak magnitudes of vertically integrated water vapor flux (IVT), which exceeded 2,100 kg s^{-1} m^{-1}, were comparably extreme (Su & Smith, 2021). Moisture transport was aided by the strengthening low-level jet ahead of Ida's extratropical low. The IVT field at 0000 UTC (Figure 5) illustrates the convergence of ingredients producing catastrophic flooding in eastern Pennsylvania and New Jersey.

4. Extreme Rainfall and Flooding

In this section, we examine rainfall and flooding, documenting the most extreme magnitudes associated with the remnants of Ida. We organize analyses in this section (and analyses in Section 5) around three geographic regions—central New Jersey, eastern Pennsylvania, and northern New Jersey. We begin with the central New Jersey region, which includes the core of peak rainfall shown in Figure 1. The central New Jersey region also includes rain gauge stations with the most extreme sub-daily rainfall accumulations; these stations are operated by the New Jersey Rutgers Weather Network and USGS. Flooding in eastern Pennsylvania, New Jersey and New York resulted in 51 flood fatalities, with 29 in New Jersey.

Storm total rainfall based on the bias-adjusted K_{DP} rainfall fields for the Central New Jersey region reached 260 mm between the watershed boundaries of the Neshanic River and Stony Brook (Figure 6). The period of peak rainfall extended from approximately 22 UTC on 1 September to 01 UTC on 2 September. Rainfall was organized along the southwest-to-northeast tracks of supercells, as detailed in Section 5. The largest rain gauge accumulation is 230 mm from a station in Hopewell, NJ, which is located in the Stony Brook watershed southeast of the core of peak rainfall (see Figure 6 for locations).

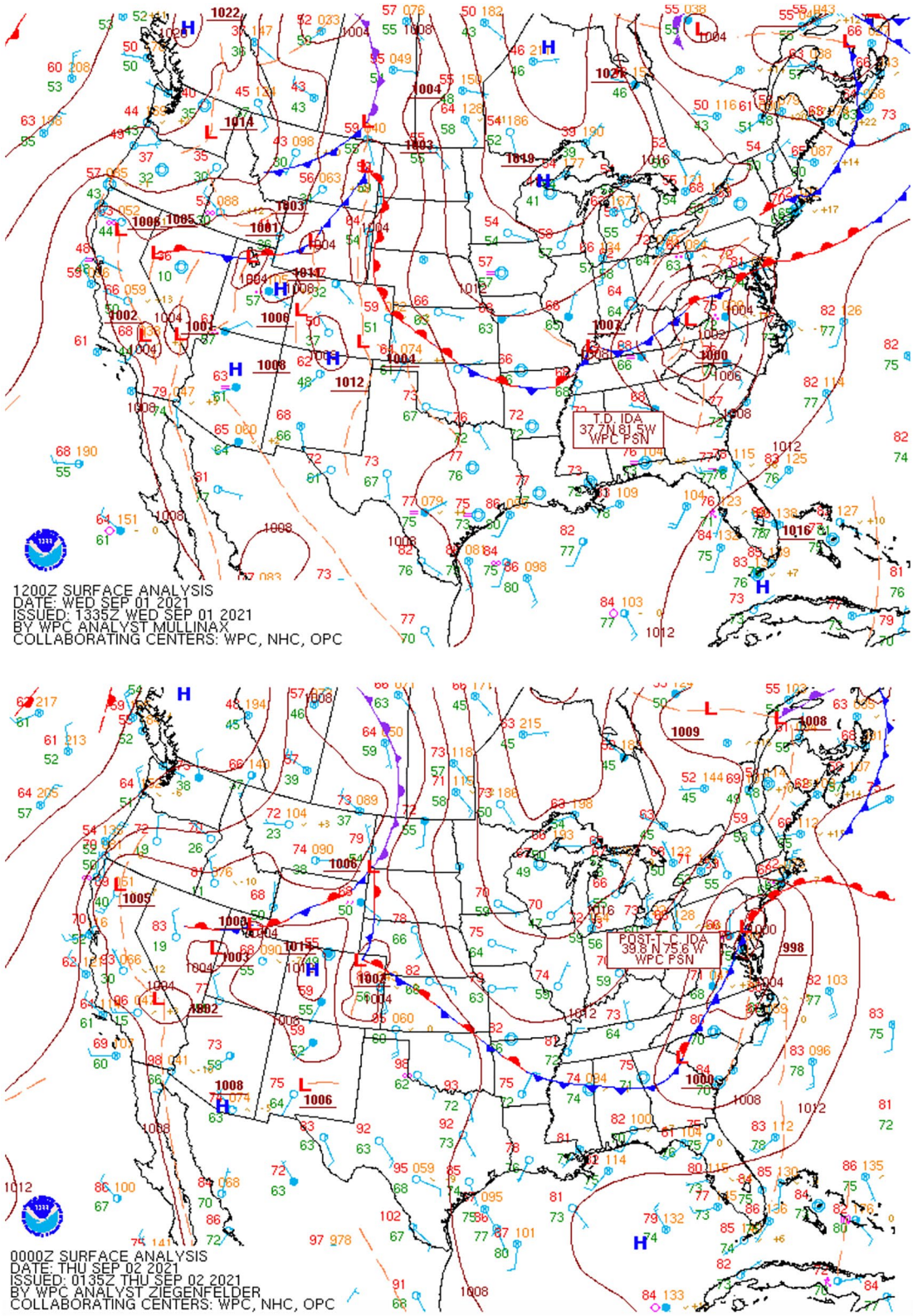

Figure 3. Storm prediction center surface analysis for 1200 UTC on 1 September (top) and 0000 UTC on 2 September (bottom).

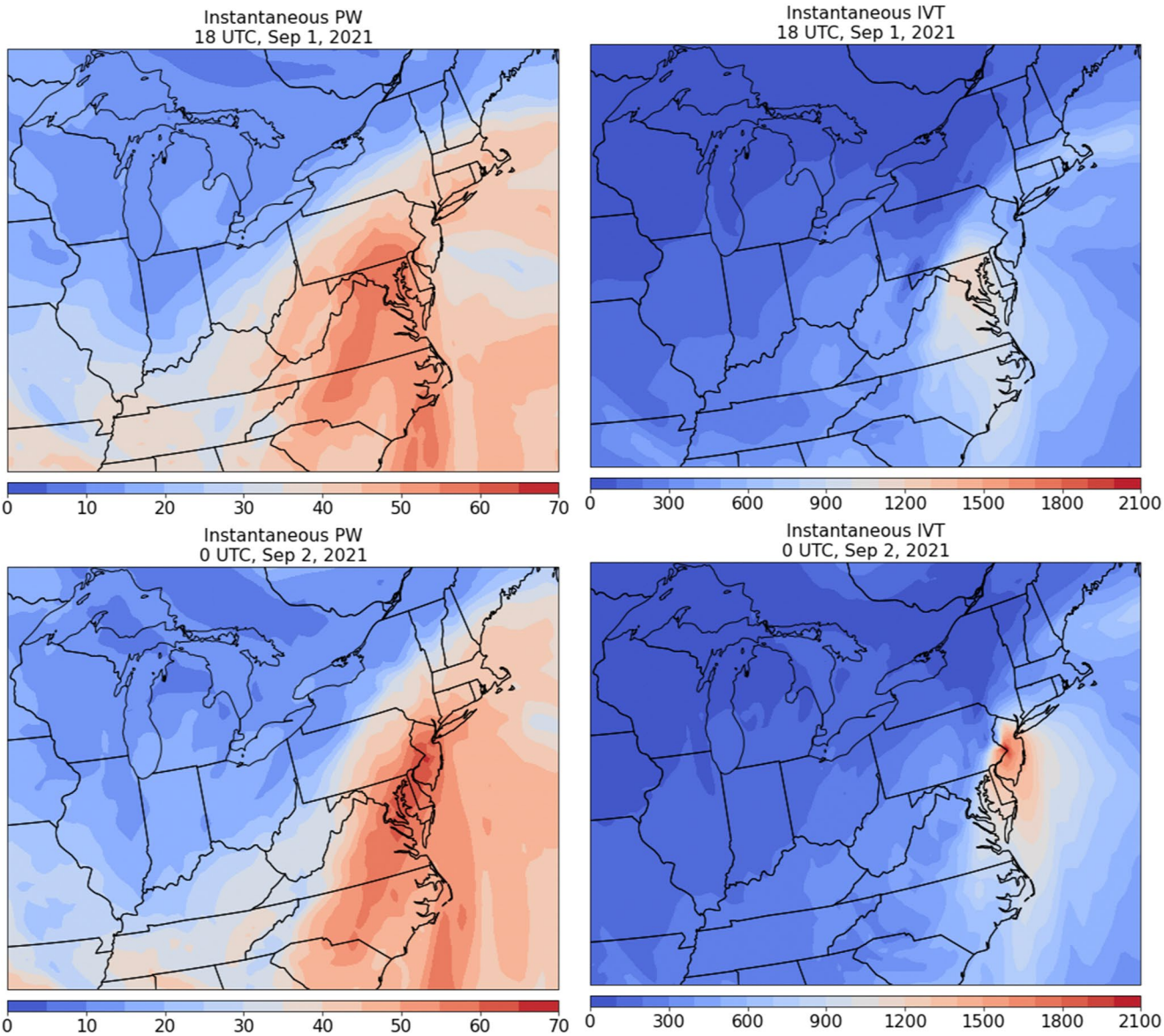

Figure 4. Precipitable water fields (mm; left column) and IVT magnitude fields (kg s^{-1} m^{-1}; right column), derived from GDAS analysis fields. The top row is for 18 UTC on 1 September 2021 the bottom row is for 00 UTC on 2 September.

Intercomparisons of rain gauge observations with K_{DP} rainfall rate time series illustrate the utility of polarimetric radar observations in resolving variability of the most intense rainfall from Ida (Figures 7 and 8). K_{DP} rainfall fields accurately capture the variability of rainfall rate at 15-min time scale. For each of the five rain gauge stations, peak 15-min rainfall rates exceed 100 mm hr^{-1}. Peak 15-min rainfall rates at Stockton around 2230 UTC (Figure 7) are from a supercell that passed over the Neshanic River basin during the following 30 min (see Section 5), producing a sharp spike of rainfall over the watershed and record flooding. The Hopewell rain gauge captures extreme short-duration rainfall (Figure 7) from supercells producing record flooding in the Stony Brook watershed.

The Skillman, Belle Mead and Hillsborough rain gauges are closely spaced along the southwest-to-northeast track of supercells (see Figure 6 for rain gauge locations). Gauge—radar intercomparisons (Figure 8) demonstrate the utility of K_{DP}-based rainfall fields in resolving fine-scale variability of extreme rainfall in space and time.

Rainfall accumulations at the Stockton, Hopewell, Skillman, Belle Mead, and Hillsborough rain gauge sites are extreme, relative to NOAA precipitation frequency values (Table 1). Observations approach 500 year return

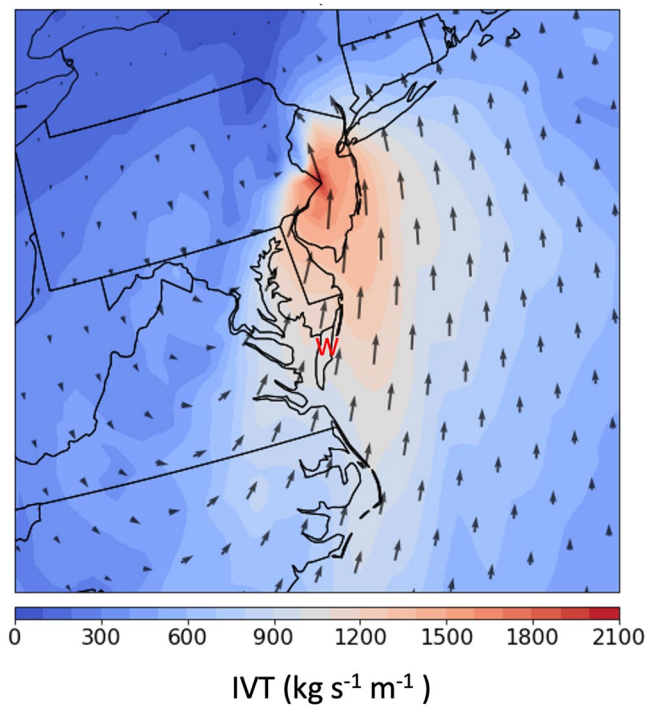

Figure 5. Vertically integrated water vapor flux field at 00 UTC on 2 September (derived from GDAS fields); length of arrows denotes the magnitude of the flux vector (kg s^{-1} m^{-1}), which is also represented by the color fill. The Wallops Island, Virginia radiosonde site is marked by a red "*W*."

interval values at 60-min time period and exceed 1000-year accumulations at 2–3 hr duration. The 3-hr accumulation of 173 mm at Belle Mead is 29 mm larger than the 1000-year return interval value.

Rain gauge observations did not, however, sample the region of peak rainfall as represented by radar rainfall fields. The peak 1-, 2-, and 3-hr rainfall accumulations based on radar rainfall fields are 106, 159, and 193 mm. The peak hourly accumulation is 9% larger than the 1000-year rainfall value; the 2-hr accumulation exceeds the 1000-year value by 23% and the 3-hr accumulation is 34% larger than the 1000-year value (Table 1). Locations of the maximum 1, 2, and 3 hr accumulations are in the region of maximum storm total accumulation extending from the boundaries of the Neshanic River to the Stony Brook watershed (Figure 6).

The peak discharge in the Neshanic River of 430 m^3 s^{-1} is 50% larger than the second ranking flood peak in a stream gaging record of more than 90 years (Figure 9; see Figure 6 for basin location). The drainage area of the Neshanic River at the USGS stream gaging station is 67 km^2. Record flooding in the Neshanic River was principally due to extreme, short-duration rainfall (Figure 9). The 5-min, basin-average rainfall rate at 2245 UTC exceeded 145 mm hr^{-1}, a remarkably large value for a 67 km^2 watershed. The sharp spike in rainfall rate over the Neshanic River watershed (Figure 9) reflects peak rainfall rates from the storm element that passed over the Stockton rain gauge from 2200 to 2230 UTC (Figure 7).

Record flooding was also recorded at the USGS stream gaging station on Stony Brook (Figure 10), which has an annual peak series of 68 years. Drainage area of the Stony Brook watershed (see Figure 6 for location) is 115 km^2. Basin average rainfall rates spiked over 90 mm hr^{-1} from supercell clusters during the period from 2245 UTC to 0015 UTC (see Section 5), producing the record flood peak of 385 m^3 s^{-1} (Figure 10).

Extreme rainfall in eastern Pennsylvania from the remnants of Ida (Figure 11), which occurred principally during the period from 1900 to 2200 UTC on 1 September, produced record flooding at numerous USGS stream gaging stations. The peak discharge of 230 m^3 s^{-1} in Valley Creek, which has a drainage area of 54 km^2, is 30% larger than the September 1999 peak from Hurricane Floyd, the second largest flood peak in the stream gaging record (Figure 12). The annual peak series for Valley Creek extends from 1983 through 2021.

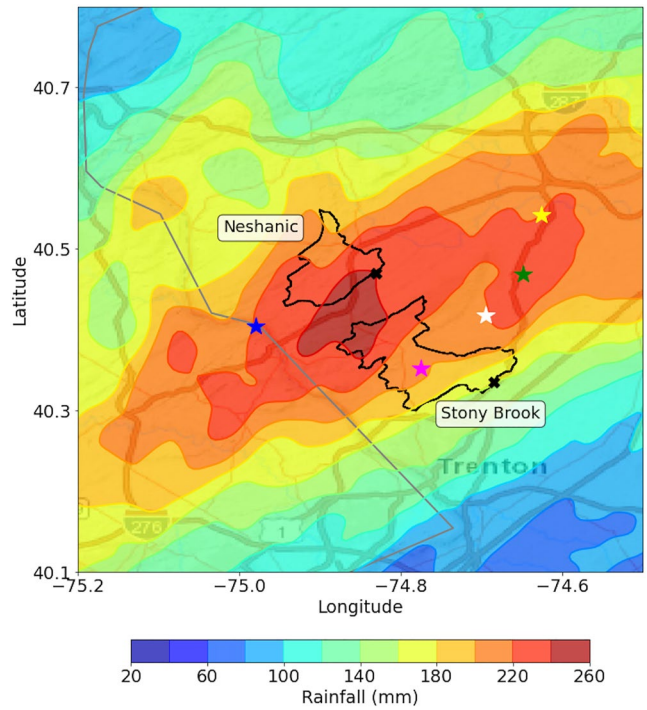

Figure 6. Storm total radar rainfall map (mm) for central New Jersey (1200 UTC on 1 September to 1200 UTC on 2 September) with Stony Brook and Neshanic basin boundaries; basin outlets are denoted by a black "*x*." Rain gauge locations for Stockton (blue star; USGS network), Hopewell (magenta star; Rutgers New Jersey Weather network), Skillman (white star; USGS network), Belle Mead (green star; USGS network) and Hillsborough (yellow star; Rutgers New Jersey Weather network) are shown (see Table 1).

Flooding in eastern Pennsylvania, like in the Neshanic River basin, was principally due to extreme, short-duration rainfall. Basin-average rainfall in Valley Creek (Figure 12 top) exhibits a sharp peak exceeding 130 mm hr^{-1} around 2130 UTC. A fast-moving supercell that tracked from southwest to northeast produced peak rainfall rates in Valley Creek (Figure 11), as detailed in Section 5.

The most extreme flooding from Ida and the largest concentration of flood fatalities occurred in northeastern New Jersey (Figure 13) and was the product of extreme rainfall, principally during the period from 23 UTC on 1 September to 02 UTC on 2 September. Multiple supercells (Section 5) produced extreme rainfall over 1–3 hr time scale and catastrophic flooding in the Elizabeth River, which has a drainage area of 44 km^2 at the USGS stream gaging station (Figure 14 top). The peak discharge of 600 $m^3\ s^{-1}$ exceeds the second largest peak by a factor of more than 3, from a stream gaging record of more than 100 years (Figure 14 bottom). The ratio of peak discharge to the sample 10-year flood is greater than 5, placing the Elizabeth River flood peak among the most extreme in the Eastern US (Smith et al., 2018).

A CoCoRaHS station north of the Elizabeth River basin (Figure 13, see also discussion in Section 5) reported a storm total accumulation of 224 mm. We time-distributed the storm total accumulation using the K_{DP}-based rainfall time series for the gauge location, yielding a 5-min time series with 224 mm accumulation and the time profile of rain rate matching the polarimetric rainfall field. The peak hourly rainfall based on this analysis is 114 mm, which is 10 mm larger than the 1000-year rainfall accumulation. The 3-hr accumulation of 191 mm is 47 mm larger than the 1000-year return interval value and just less than the maximum 3-hr accumulation of 193 mm between the Neshanic River and Stony Brook watersheds (as detailed above).

From Valley Creek in eastern Pennsylvania to the Elizabeth River in northern New Jersey, rainfall extremes and flooding are tied to striking temporal and spatial variability of rainfall, as detailed in the following section.

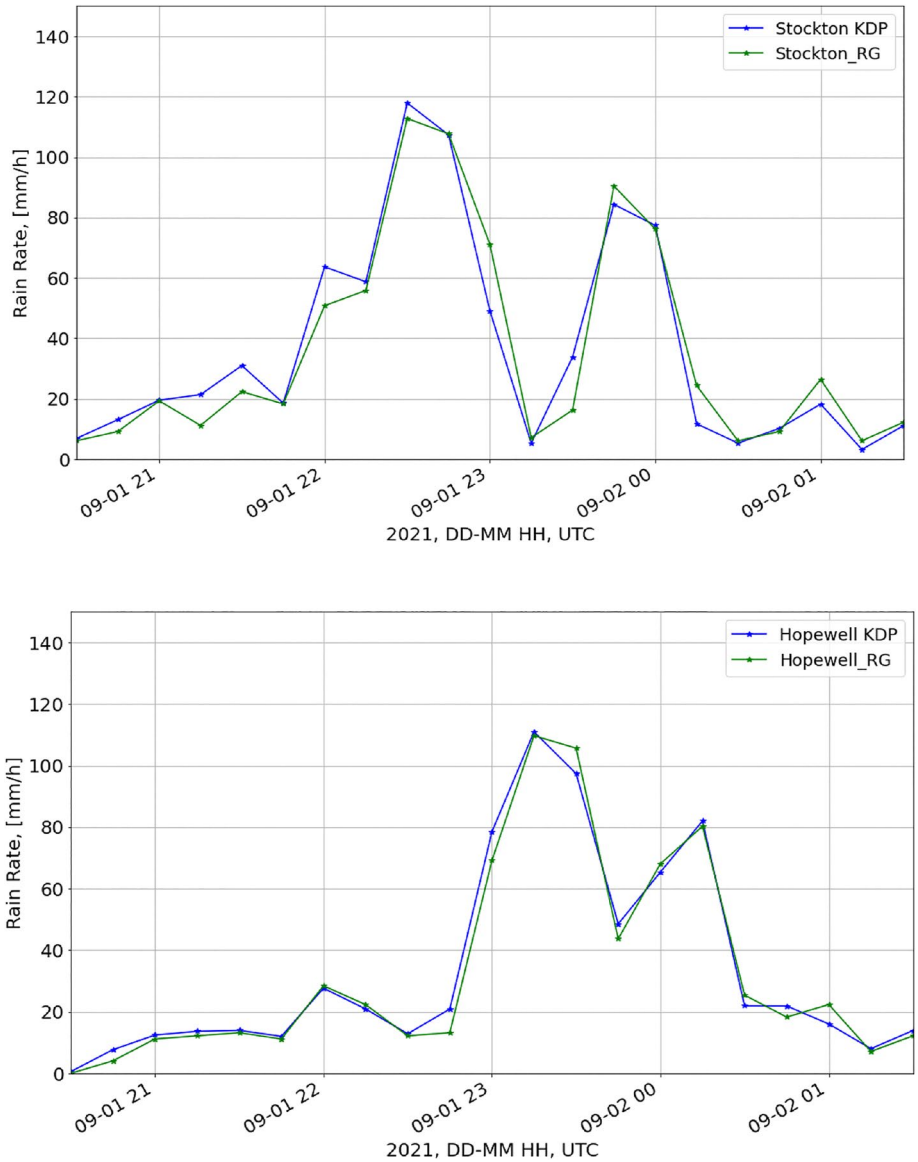

Figure 7. Time series of rain gauge and radar rainfall estimates (KDP) at the Stockton rain gauge location (top) and Hopewell rain gauge location (bottom); see Figure 6 for locations.

5. Supercells and Short-Duration Rainfall Extremes

A prominent feature of Hurricane Ida's passage through the Northeastern US was the outbreak of tornadoes in Pennsylvania and New Jersey, including the EF3 Mullica Hills tornado in New Jersey. The tornado outbreak points to the role of supercells in producing extreme rainfall from the remnants of Ida. Supercells are not an incidental piece of the story, but a central agent of extreme flooding, as detailed below.

The record flood peak in Valley Creek (Figure 12) was produced by extreme short duration rainfall, with peak rainfall rates exceeding 200 mm hr^{-1} in the eastern portion of the watershed at 2117 UTC on 1 September (Figure 15). A supercell passing southeast of the watershed was the agent of extreme rainfall—mesocyclone locations (based on storm rotation analyses; see Section 3) are shown for the period 2111–2129 UTC in Figure 15. Shortly after the peak rainfall in Valley Creek, the Fort Washington tornado (EF2) formed northeast of the watershed. Location of the tornado at 2135 UTC is denoted by the downward black triangle in Figure 15.

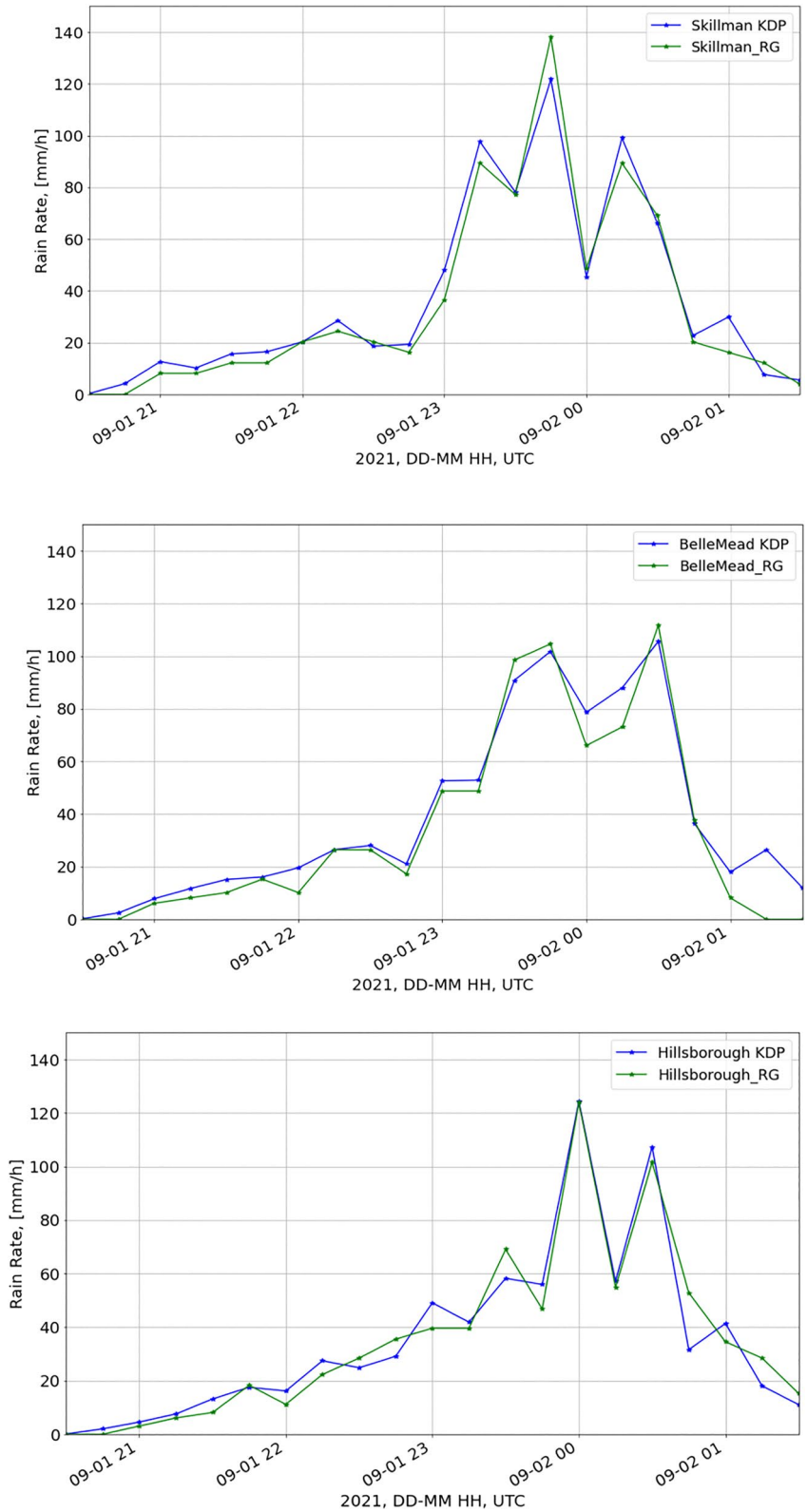

Figure 8. Time series of rain gauge and radar rainfall estimates (KDP) at Skillman (top), Belle Mead (middle) and Hillsborough (bottom); see Figure 6 for locations.

Table 1
Maximum Rainfall (mm) at 60, 120, and 180 min Time Scale for Ida and NOAA Precipitation Frequency Results

Station	60 min	120 min	180 min
Stockton	87	134	163
Hopewell	87	134	163
Skillman	88	142	163
Belle Mead	89	147	173
Hillsborough	87	134	163
NOAA 200	81	104	116
NOAA 1000	97	129	144

Note. Rain gauge locations are shown in Figure 6. The NOAA 200 row provides 200-year return interval rainfall values; the NOAA 1000 row presents 1000-year return interval values.

Storm motion and evolution resulted in striking spatial variability of rainfall, as illustrated through rain rate fields at 2113, 2115, 2117, and 2119 UTC (Figure 16) and time series of storm properties from 2100 to 2145 UTC (Figure 17). Structure of the rain rate fields reflects the evolving dynamical and microphysical processes in the forward flank downdraft of the supercell (Markowski & Richardson, 2011). Peak rain rate in the supercell increases sharply from 150 mm hr^{-1} at 2100 UTC to its peak at 2117 UTC exceeding 200 mm hr^{-1}. Peak rain rate decreased briefly from the 2117 UTC peak, but returned to values close to 200 mm hr^{-1} at 2128 UTC, immediately preceding first reports of the Fort Washington Tornado. Paired with the period of peak rain rates is a rapid increase in the area with extreme rain rates; from 2113 to 2128 UTC the area with rain rates greater than 150 mm hr^{-1} plateaus above 60 km^2 (Figure 17). Sharp increases in extreme rainfall prior to 2113 UTC and sharp decreases in extreme rainfall after 2128 UTC characterize the evolving structure of the supercell. Spinup and decay of the mesoscyclone

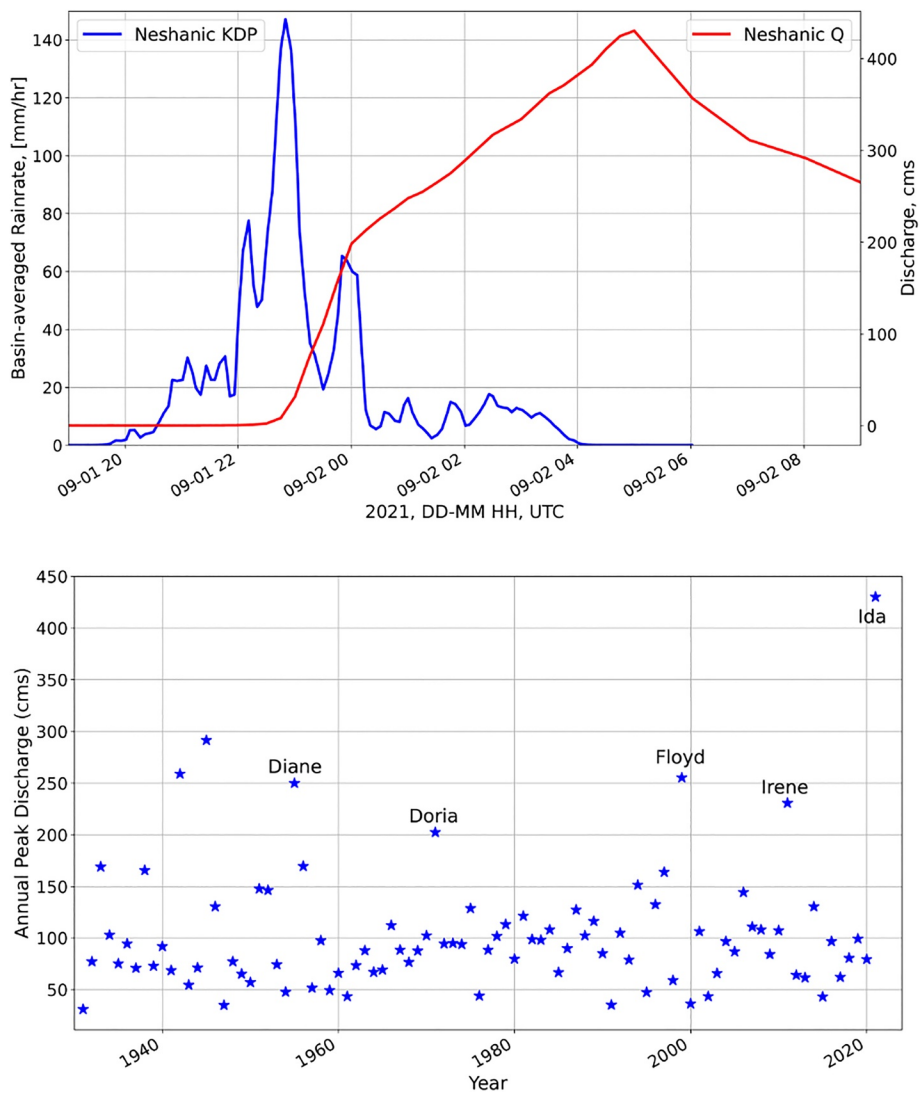

Figure 9. Basin-average rain rate (blue) and discharge (red) time series for the Neshanic River; 1 September 1900 UTC to 2 September 0900 UTC (top panel). Annual flood peaks (m^3 s^{-1}) for the Neshanic River are shown in the bottom panel.

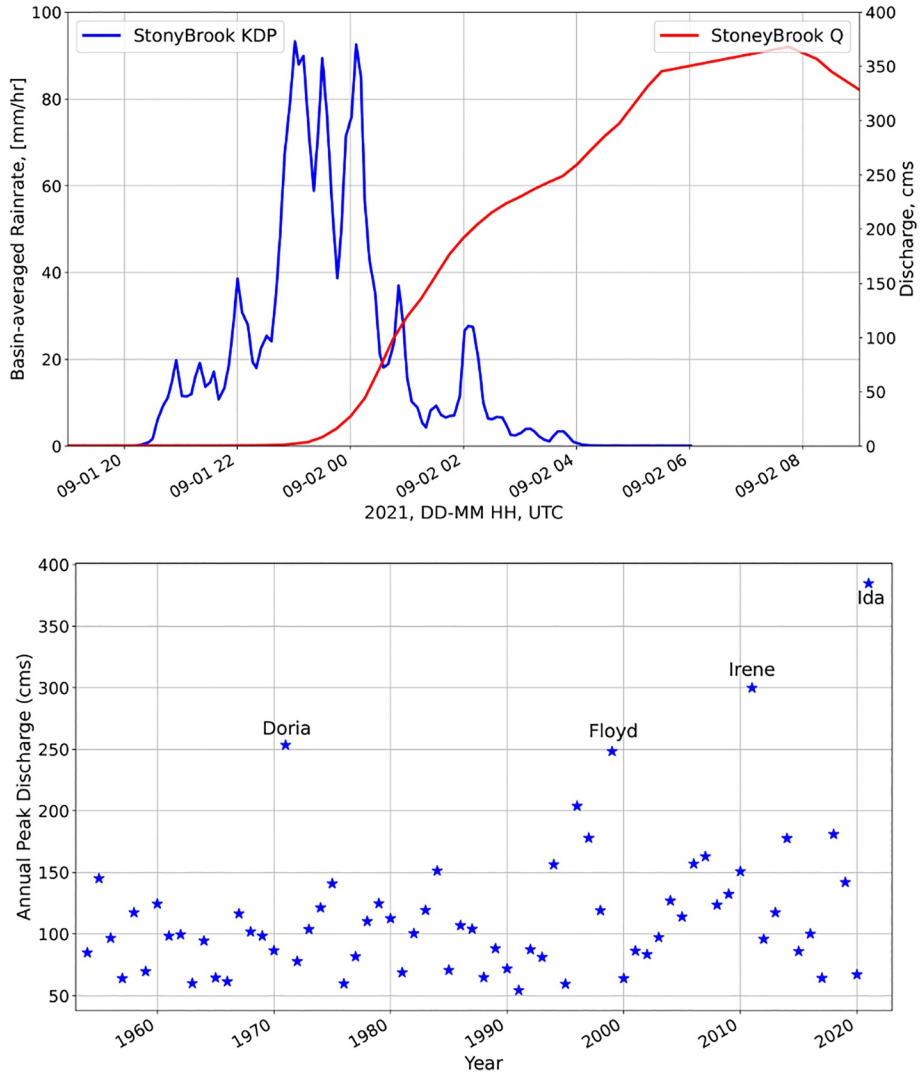

Figure 10. Basin-average rain rate (blue) and discharge (red) time series for Stony Brook; 1 September 1900 UTC to 2 September 0900 UTC (top panel). Annual flood peaks ($m^3\ s^{-1}$) for Stony Brook are shown in the bottom panel.

likely contributed to rain rate variability over the period from 2100 to 2145 UTC and the large spatial gradients in rainfall over the region (Figure 11).

Size of the supercell rain area is a key feature of extreme flooding in Valley Creek (Figure 17) and other watersheds experiencing record floods in Pennsylvania and New Jersey. At 2117 UTC, the area with rain rates greater than 100 mm hr^{-1} was larger than 250 km^2 and the 150 mm hr^{-1} rain area exceeded 70 km^2. As noted above, the area exceeding 150 mm hr^{-1} increased sharply, plateaued for a brief period and decreased sharply. The rain area exceeding 100 mm hr^{-1} shows less variability—the area exceeded 170 km^2 at 2100 UTC and 190 km^2 at 2145 UTC.

Storm motion for the supercell as it approached and passed through the Valley Creek watershed was to the northeast at approximately 15 m s^{-1} (based on storm tracking analyses using reflectivity centroids). For the 2-min time step of rainfall fields in Figure 16, storm motion implies a translation of approximately 2 km to the northeast. Elements of rainfall variability that control the sharp spike in basin-average rainfall rate and record flooding in Valley Creek (Figure 12) can be characterized by structure, motion and rainfall evolution of the supercell.

Record flooding for the Neshanic River in central New Jersey (Figure 9) also resulted from extreme, short-duration rainfall. A supercell tracking southeast of the basin from 2230 to 2300 UTC on 1 September (upward red triangles in Figure 18 denote locations of the mesocyclone) produced a sharp spike in basin-average rainfall rates, with a peak value exceeding 140 mm hr^{-1} at 2244 UTC (Figure 9). The supercell produced 15-min rainfall rates

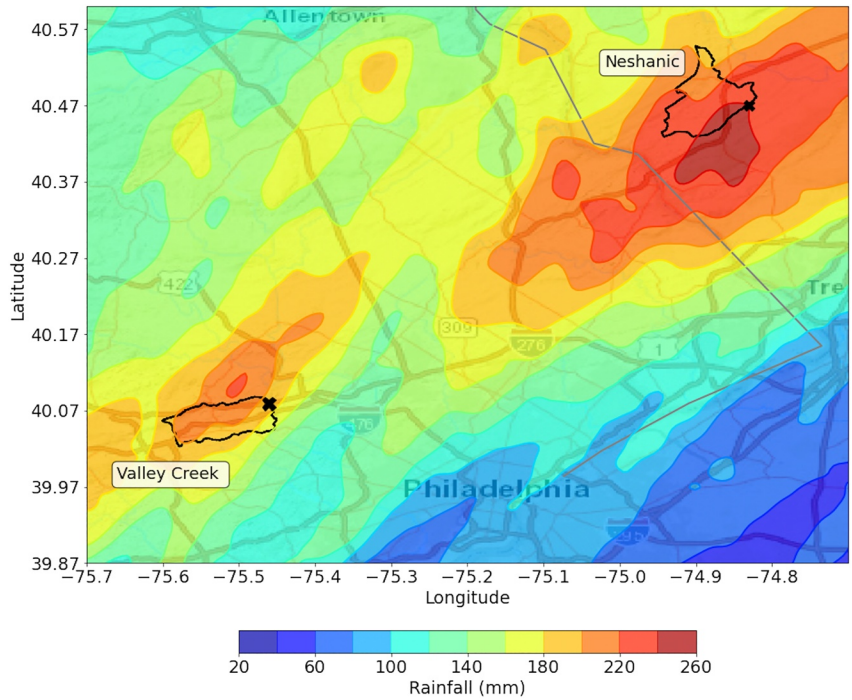

Figure 11. Storm total radar rainfall map (mm) for eastern Pennsylvania (1200 UTC on 1 September to 1200 UTC on 2 September) with Valley Creek and Neshanic River basin boundaries. Basin outlets are denoted by black "*x*."

of 120 mm hr^{-1} at the Stockton rain gauge (Figure 7) prior to passing over the Neshanic River watershed (see Figure 18 for location of the Stockton rain gauge). The Upper Makefield Tornado (EF1) passed to the southeast of the watershed from 2230 to 2235 UTC (denoted by the downward black triangle in Figure 18).

At 2244 UTC, rainfall rates exceeding 150 mm hr^{-1} covered much of the Neshanic River basin (Figure 18). Unprecedented flooding in the Neshanic River (Figure 9) was fundamentally tied to the footprint of extreme rainfall rates from the supercell that tracked over the region from 2230 to 2300 UTC. The area with rain rates greater than 150 mm hr^{-1} approached 80 km^2 for the supercell; the area with rainfall rates exceeding 100 mm hr^{-1} peaked at 350 km^2. These values are somewhat larger than peak values from the supercell that produced extreme flooding around Valley Creek (Figure 17).

Storms producing extreme rainfall and flooding from Valley Creek to the Neshanic River were elements of a long-lived cluster of supercells that moved through eastern Pennsylvania into New Jersey from 2100 to 2300 UTC (Figures 11, 15, and 18). The large variability in rainfall over the region was driven by motion and evolution of the supercell clusters. During the period from 2100 to 2300 UTC, supercells moved rapidly from southwest to northeast, based on tracking locations of low-level reflectivity centroids. Storm speed ranged from 10 to 15 m s^{-1} with higher speeds on the southwest end of the domain and lower speeds on the northeast end of the domain in New Jersey. Slower storm motion over New Jersey contributed to the larger accumulations in the region (Doswell et al., 1996). The area covered by extreme rainfall was exceptionally large, with somewhat larger values on the northeast end of the supercell track (Figures 15 and 18).

Record flooding in the Stony Brook resulted from a sequence of supercells during the period from 2230 UTC on 1 September to 0030 UTC on 2 September, each producing spikes of basin-average rain rate exceeding 90 mm hr^{-1} over the 115 km^2 watershed (Figure 10). Peak rain rates over Stony Brook at 2330 UTC (Figure 19) were paired with the Princeton tornado (EF1), the last of the day. Extreme rainfall and the Princeton tornado were produced by a long-lived supercell that had spawned the Mullica Hill tornado (EF3) in southern New Jersey around 2210 UTC on 1 September.

The core of peak rainfall at 2330 UTC (Figure 19) was located between the Hopewell rain gauge to the southwest and the Skillman rain gauge to the northeast. The largest 15-min rainfall rates at the Hopewell rain gauge occurred

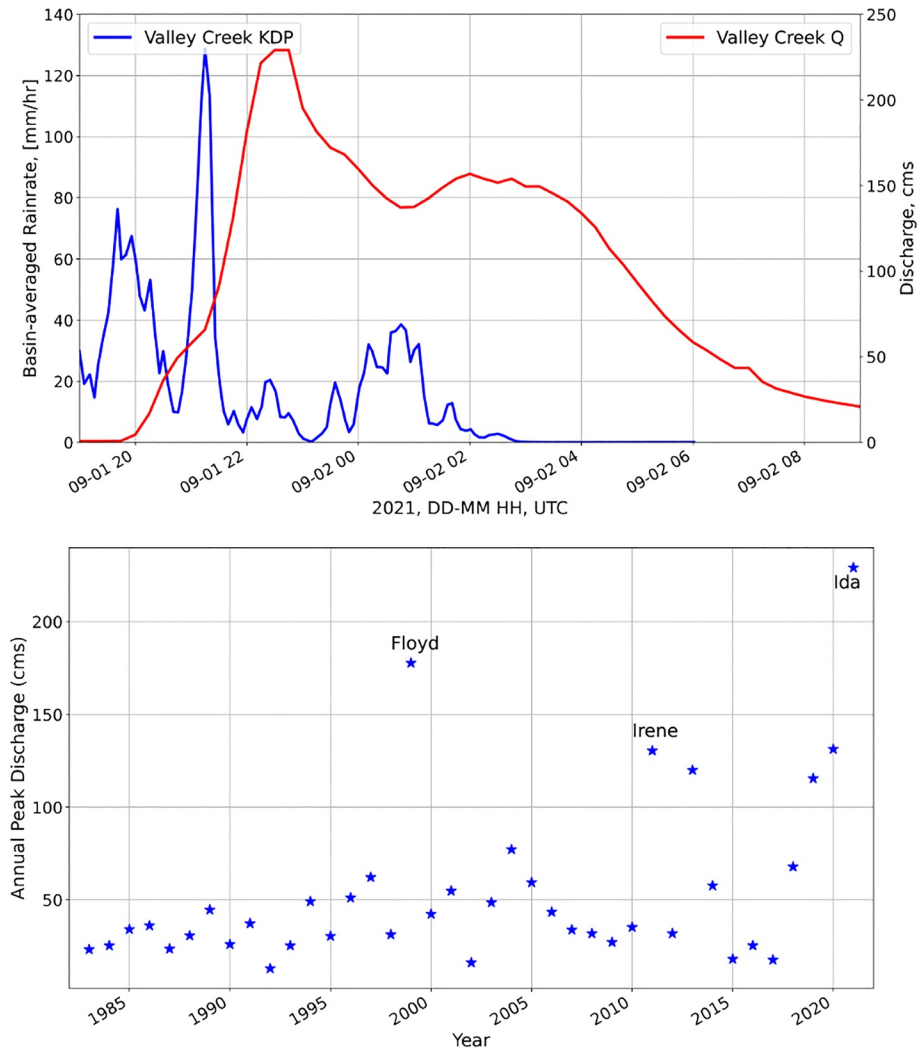

Figure 12. Basin-average rain rate (blue) and discharge (red) time series for Valley Creek; 1 September 1900 UTC to 2 September 0900 UTC (top panel). Annual flood peaks ($m^3\ s^{-1}$) for Valley Creek are shown in the bottom panel.

during the preceding 30 min (Figure 7). The 140 mm hr^{-1} peak rain rate at the Skillman rain gauge (Figure 8) covered the 15 min period following 2330 UTC, as the supercell moved to the northeast (Figure 19). Flood response in Stony Brook was tied to striking spatial variability in rainfall over the watershed during the periods of peak rain (Figure 19). Gauge-radar intercomparisons illustrate the utility of K_{DP}-based rainfall fields in resolving spatial and temporal variability of rainfall extremes over Stony Brook—sized watersheds.

Over the course of the afternoon and evening, the number of supercells increased as the focus of flooding shifted to New Jersey and New York. At 2330 UTC, there were five supercells identified by storm rotation in central New Jersey and eastern Pennsylvania; these storm elements were responsible for peak rain rates throughout the region. Clustering of supercells occurred throughout the day, organized in part by the evolution of the warm front that pushed into central New Jersey and the cold front, that extended from southeastern Pennsylvania into the Southeastern US by 00 UTC on 2 September (Figure 3). The striking convergence of water vapor flux over central New Jersey (Figure 5) set the stage for unprecedented rainfall and flooding from clusters of supercells.

Catastrophic flooding in the Elizabeth River resulted from a sequence of supercells that tracked over the watershed from 2300 to 0100 UTC on 2 September (Figure 14). The most extreme rainfall, with basin-average rain rates approaching 110 mm hr^{-1}, occurred around 0038 UTC (Figure 20). The track of the supercell along the eastern margin of the basin is shown in Figure 20.

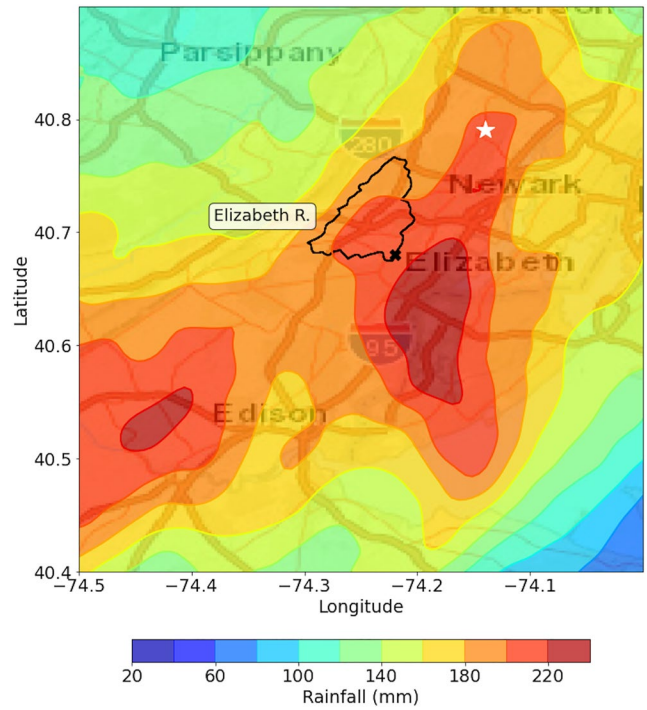

Figure 13. Storm total rainfall map (mm) for northern New Jersey (1200 UTC on 1 September to 1200 UTC on 2 September) with the Elizabeth River basin boundary and location of the North Arlington CoCoRaHS rain gauge (white star).

Clusters of supercells in New Jersey produced some of the largest short-duration and storm total rainfall accumulations from Ida (Section 4). A supercell passed over the North Arlington CoCoRaHS station around 0030 UTC on 2 September (Figure 20) producing the reconstructed hourly rainfall accumulation of 114 mm, as detailed in the previous section. Earlier, this storm element produced extreme rainfall rates over the Elizabeth River watershed. Tracks of supercells moved to the east after 0030 UTC, triggering devastating flooding in New York City.

Further south and earlier on 1 September, a long-lived supercell produced a narrow line of 75–100 mm rainfall extending from near Charlottesville, Virgina to Baltimore, Maryland, a distance of more than 300 km (red circles in Figure 1). The Virginia-Maryland storm system reflects the early phase of extreme rainfall on 1 September when a single supercell track is responsible for extreme flooding. The first fatality of the day occurred in Rockville, Maryland during the early morning when a basement apartment was flooded, presaging events late in the day in New York City.

Supercells were the dominant agents of extreme rainfall and flooding in the Northeastern US on 1–2 September. Attributes that contributed to the unprecedented rainfall include size, motion and evolution of individual supercells and diverse modes of clustering of supercells. Tracks of multiple supercells along a similar path were an important aspect of record 1–3 hr rainfall accumulations. The life cycles of supercells and their mesocyclones contributed to the pulsating nature of extreme rainfall (Smith et al., 2019) and spatial variability of the most severe flood impacts.

6. Discussion

"Mixtures" of distinct flood types have been viewed as important aspects of the upper tail of flood peaks, dating back to the development of hydrometeorological tools for engineering design by Arthur Morgan and Miami Conservancy engineers (Morgan, 1917; for more recent developments, see Hirschboeck, 1987; Merz & Blöschl, 2003; Miniussi et al., 2020; Smith et al., 2011, Villarini, 2016). Mixtures of flood types are a prominent feature of annual peak distributions for the eastern United States, with tropical cyclones standing out as principal agents of extreme floods (Villarini & Smith, 2010). How does Ida fit into a mixtures framework for assessing the upper tail of flood peaks and short-duration rainfall?

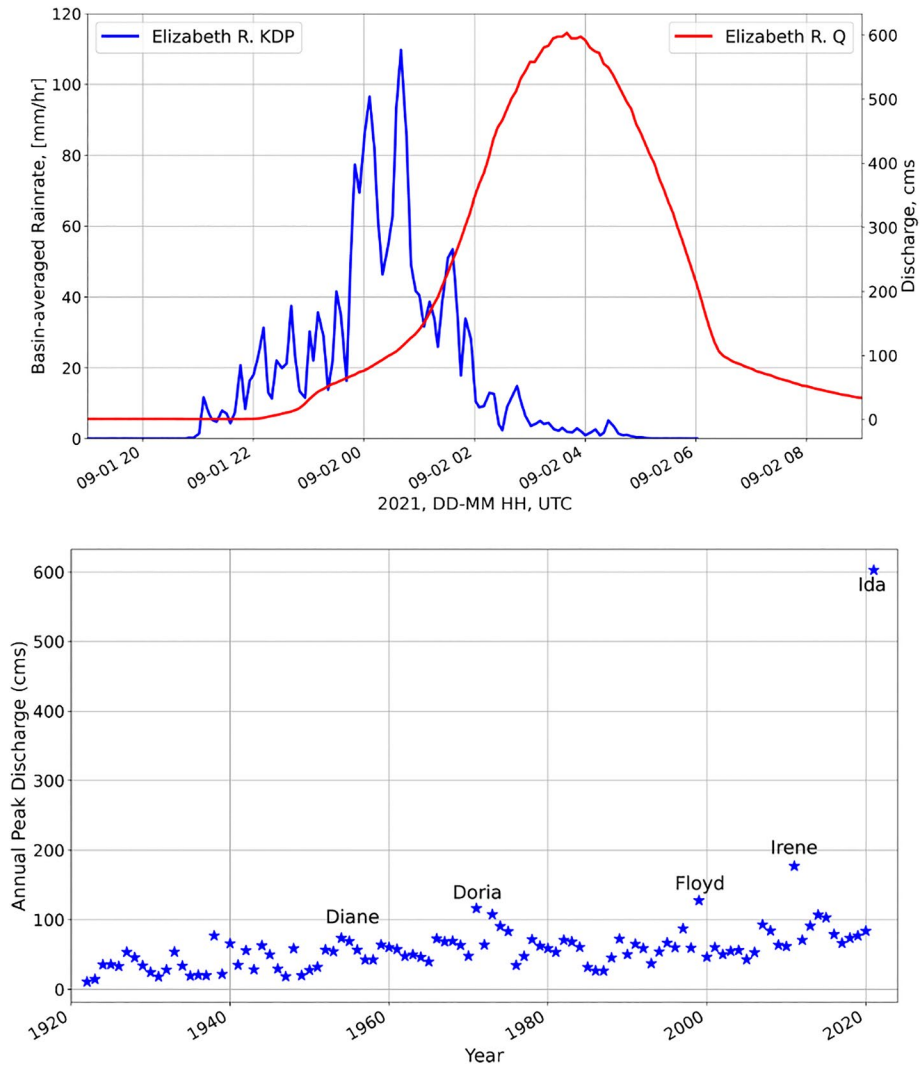

Figure 14. Basin-average rain rate (blue) and discharge (red) time series for Elizabeth River; 1 September 1900 UTC to 2 September 0900 UTC. Annual flood peaks (m^3 s^{-1}) for the Elizabeth River are shown in the bottom panel.

Six tropical cyclones—Diane (1955), Doria (1971), Agnes (1972), Floyd (1999), Irene (2011), and Ida (2021) are responsible for many of the largest flood peaks at USGS stream gaging stations in eastern Pennsylvania and New Jersey (e.g., Figures 9, 10, 12, and 14). Extratropical Transition is a key element of extreme rainfall and flooding, with Agnes, Floyd and Irene providing the material for previous studies of Extratropical Transition and flooding (Atallah & Bosart, 2003; Colle, 2003; DiMego & Bosart, 1982; Jung & Lackmann, 2019; Liu & Smith, 2016; Liu et al., 2020; Matyas, 2017).

Table 2
Maximum 60-Minute Increase in Discharge (m^3 s^{-1} hr^{-1}) for Ida, Irene and Floyd From Valley Creek, Neshanic River, Stony Brook, and Elizabeth River

Basin	Ida	Irene	Floyd
Valley	82	54	27
Neshanic	167	63	NA
Stony Brook	92	56	49
Elizabeth	88	44	37

Rainfall from tropical cyclones that undergo Extratropical Transition along the East Coast, however, exhibit contrasting spatial and temporal distributions (Atallah et al., 2007; Bailey et al., 1975; Matyas, 2017; United States Weather Bureau, 1955; Villarini et al., 2011). A feature that distinguishes Ida from the other five tropical cyclones is concentration of rainfall extremes during short durations. This conclusion is supported by rainfall and discharge observations from each of the storms (as detailed above; the most comprehensive summary of short-duration rainfall observations from tropical cyclones is presented in AWA (2019)). The flood peaks from Ida are larger than peaks from the other five storms and the response times are more rapid. In Table 2, the maximum 1-hr rate of increase in discharge in Valley Creek, Neshanic

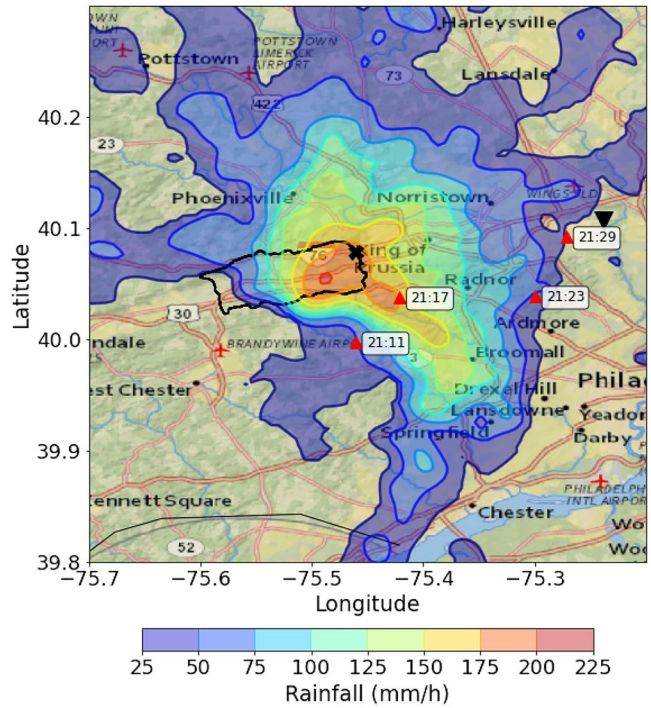

Figure 15. Radar rain rate field (mm hr^{-1}) at 2117 UTC on 1 September with Valley Creek basin boundary and mesocyclone locations at 2111, 2117, 2123, and 2129 UTC (red triangles). Inverted black triangle shows location of the Fort Washington tornado (EF2) at 2135 UTC. Black "*x*" marks location of the Valley Creek basin outlet.

River, Stony Brook and the Elizabeth River are compared for Hurricanes Floyd (1999), Irene (2011) and Ida (2021). The maximum 1-hr rate of increase provides a quantitative tool for assessing rise times of flood hydrographs (see also Saharia et al., 2017). For each of the watersheds, short-duration rainfall extremes from Ida result in the most rapid rise times. In Stony Brook, for example, the peak value is 92 $m^3\ s^{-1}$ per hour for Ida, 56 $m^3\ s^{-1}$ per hour for Irene and 49 $m^3\ s^{-1}$ per hour for Floyd.

The 1 September 1940 Ewan, New Jersey storm, which produced record 24-hr rainfall (610 mm) for New Jersey (Schoner & Molansky, 1956; Schreiner & Riedel, 1978; U.S. Army Corps of Engineers, 1973), illustrates the challenges of storm classification. Extreme rainfall was linked to moisture from Hurricane 4 (1940), which was located approximately 500 km southeast of the region of extreme rainfall (see Galarneau et al., 2010 for discussion of "predecessor" rainfall events ahead of tropical cyclones). Schoner and Molansky (1956) note that "although there was a tropical cyclone located some distance off the Virginia coast during the period of heavy rain… storm precipitation was more directly associated with a very slow moving cold front." The 1940 Ewan, New Jersey storm is classified as a "local" storm in the 2018 PMP study for Pennsylvania (AWA, 2019). For PMP studies, the local classification is principally used for organized convective storms. The 610 mm accumulation at Ewan was based on a bucket survey measurement, so there is no direct evidence for short-duration accumulations. Time distribution of rainfall in the US Army Corps of Engineers storm catalog (U.S. Army Corps of Engineers, 1973) points to accumulations at sub-daily time scales that are comparable to the peaks from Ida.

Rainfall extremes for the six tropical cyclones—Diane, Doria, Agnes, Floyd, Ireane and Ida—are paired with extremes of atmospheric water balance components. Precipitable water at 00 UTC on 2 September from the Wallops Island, Virginia sounding, which is located upstream of the New Jersey flood region (see location in Figure 5) was 57 mm. Comparably large values of precipitable water characterized the other five tropical cyclones (based on 20th Century Reanalysis fields). Extremes of the atmospheric water balance are an important piece of the tropical cyclone role in determining the upper tail of flood peak distributions, but they do not provide sharp contrasts between Ida and other tropical cyclone floods in the region.

CAPE from the Wallops Island sounding at 00 UTC on 2 September was 1,130 J kg^{-1} (based on virtual temperature). Storm Prediction Center analyses show values of CAPE greater than 2,000 J kg^{-1} preceding the period of

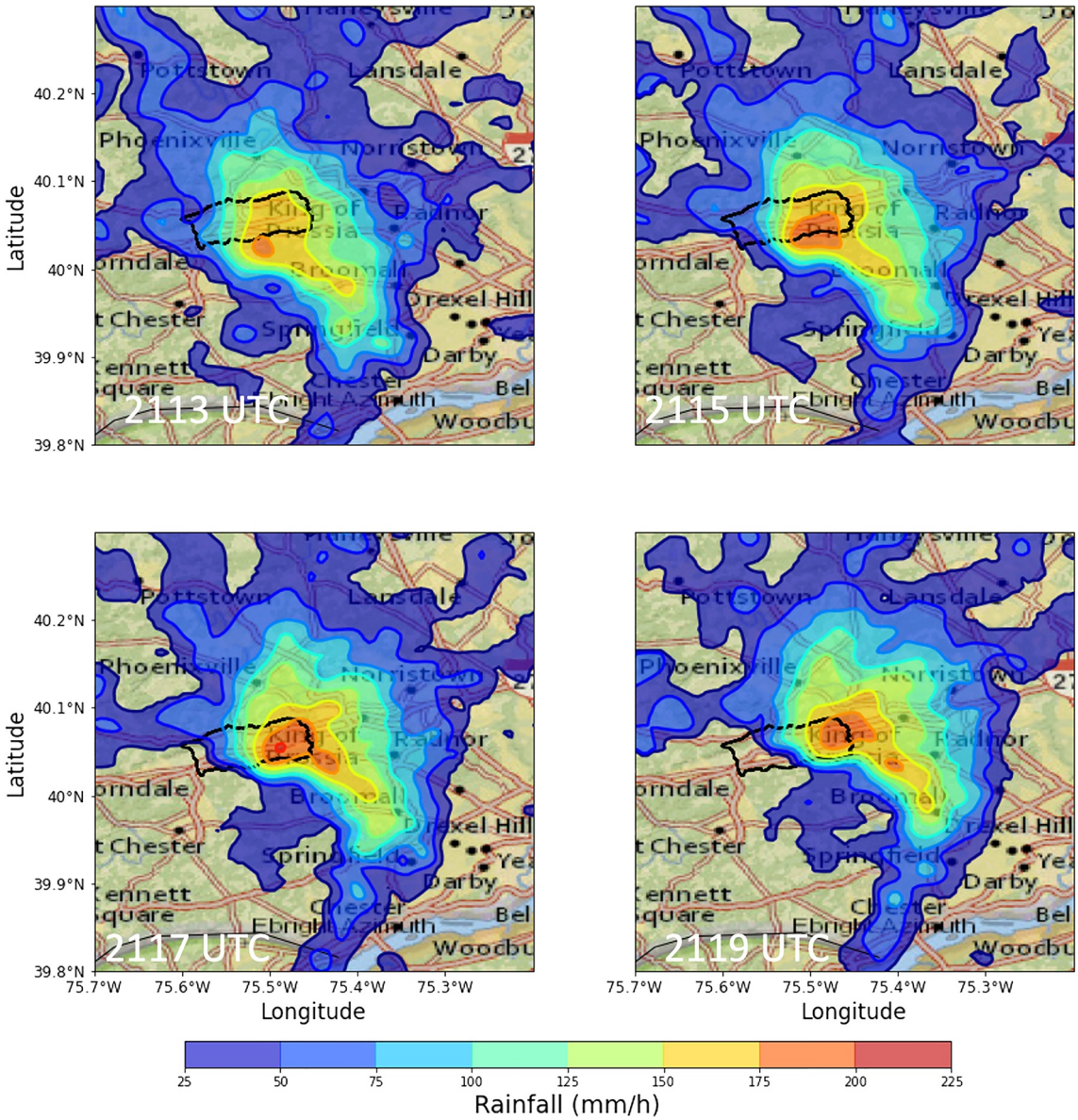

Figure 16. Radar rain rate fields (mm hr^{-1}) at 2113 UTC (upper left), 2115 UTC (upper right), 2117 UTC (lower left) and 2119 UTC (lower right) on 1 September with Valley Creek basin boundary in black.

peak rainfall in central New Jersey. Temperature and moisture advection by the low level jet east of the developing cold front created a storm environment with both large values of precipitable water and CAPE for the remnants of Ida. For the non-Ida storms, CAPE values from 20th Century reanalysis fields have peak values less than 200 J kg^{-1}. Available evidence suggests that large values of CAPE distinguish Ida from Diane, Doria, Agnes, Floyd, and Irene. Additional analyses of CAPE fields for previous storms and for tropical cyclones in a warming environment (e.g., Liu et al., 2017) can provide guidance on the role of CAPE for extreme short-duration rainfall from Ida-like storms.

Supercells are the key ingredient of extreme rainfall from Ida. From the storm environment perspective, the extra-tropical element of Extratropical Transition creates a setting not unlike that of a Southern Plains severe weather outbreak (Figure 3) and the tropical element introduces water vapor that exceeds Southern Plains norms. Size, motion and organization of supercells all contribute to creating the distribution of extreme rainfall from Ida.

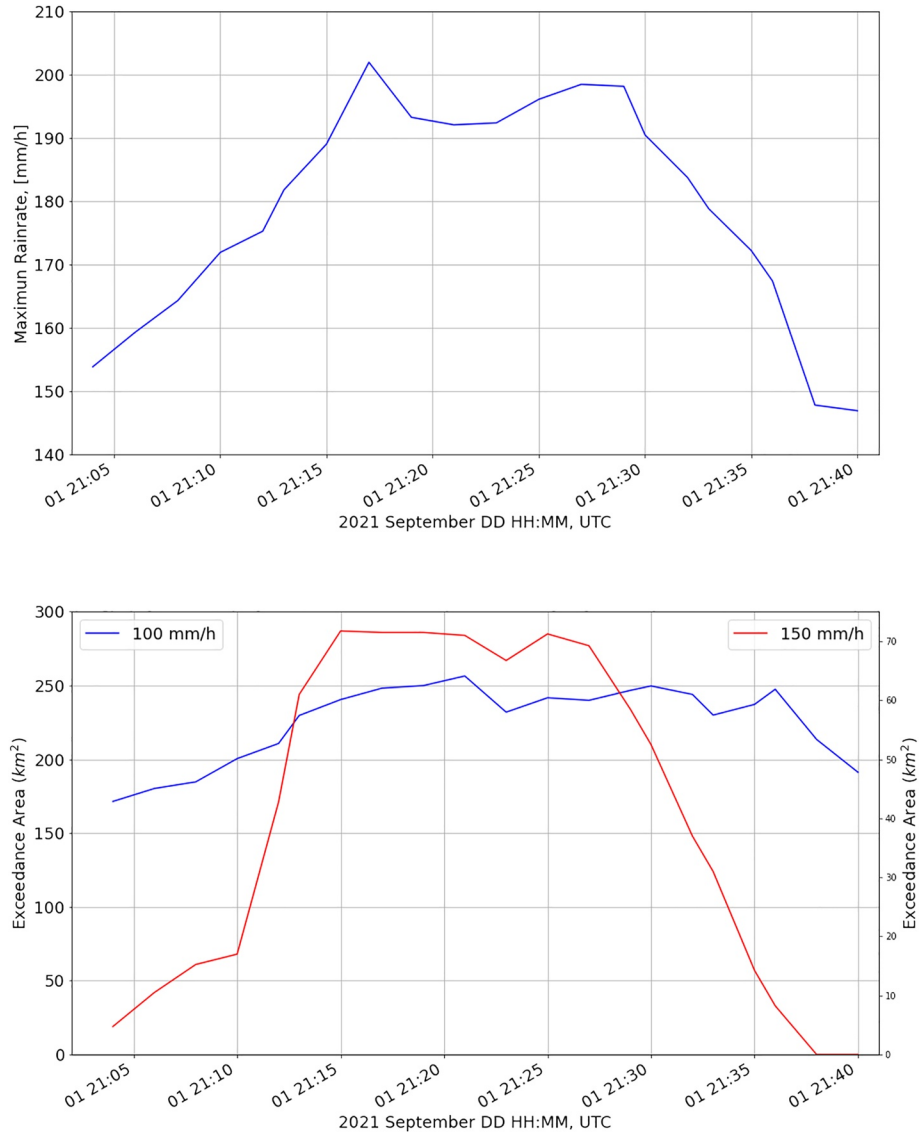

Figure 17. Time series of peak rainfall rate for the supercell shown in Figures 15 and 16 (top); the bottom panel shows the area with rainfall rates exceeding 100 mm hr^{-1} (left axis) and 150 mm hr^{-1} (right axis).

Polarimetric radar studies have been used to distinguish tornadic from non-tornadic supercells (Kumjian & Ryzhkov, 2008; M. S. Van Den Broeke, 2020). Less attention has been devoted to assessing polarimetric signatures of extreme rainfall from supercells. Lessons from the tornado literature can inform extreme rainfall studies. Analyses of updrafts and downdrafts through Z_{DR} and K_{DP} columns (Kumjian, 2013) should provide insights to the water balance of storms. Polarimetric studies of low-level K_{DP} features (Romine et al., 2008) provide a backdrop for assessing processes controlling the size of the extreme rain area of supercells. Doppler radar analyses of rotational motion can provide insights to proposed mechanisms for amplifying rainfall in supercells and mesovortices (Nielsen & Schumacher, 2020a).

For Ida, the hydrometeor classification in areas of extreme rainfall was predominantly hail with rain. Negative buoyancy in downdrafts can amplify rain rates through its effects on vertical motion. Evaporating rain and melting hail and graupel can both induce negative buoyancy that can contribute to extreme rain rates in downdrafts. For the near-saturated conditions in Ida, melting of mixed phase hydrometeors is likely an important source of negative buoyancy. Descending K_{DP} columns provide a potentially useful polarimetric signature of downdraft-driven rainfall extremes (Kuster et al., 2021; see also Kumjian et al., 2010; Romine et al., 2008; Trapp et al., 2017). The

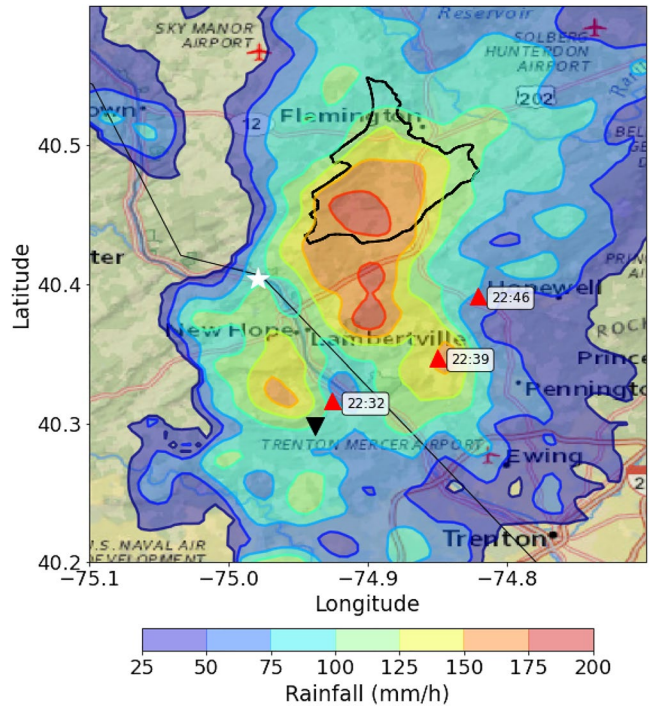

Figure 18. Radar rain rate field (mm hr^{-1}) at 2244 UTC on 1 September with Neshanic River basin boundary and mesocyclone locations at 2232, 2239, and 2246 UTC (red triangles). Inverted black triangle shows location of the Upper Makefield tornado (EF1) at 2230 UTC. White star marks location of the Stockton NJ rain gauge (Table 1).

tropical aspect of the storm environment contributed to a deep layer of humidity, a typical setting for extreme rainfall from warm rain processes. The combination of efficient warm rain processes and mixed phase processes strengthening downdrafts through melting hail and graupel provides an environment supporting extreme rain rates.

Polarimetric measurements provide rainfall estimates that capture key elements of rainfall variability, but a significant bias adjustment based on rain gauge observations is necessary; the multiplicative bias is 1.4 for Ida. It would be useful to better understand the physical processes that result in significant bias in extreme rainfall estimates based on polarimetric measurements. Three factors warrant additional consideration. Emerging research suggests that the pre-factor in R(K_{DP}) relationships is quite variable depending on the type of raindrop size distributions (A. Ryzhkov et al., 2022). Pre-factors are generally higher for tropical ("warm") rain dominated by smaller raindrops and they are smaller for continental ("cold") rain with an abundance of large raindrops that originate from melting graupel and hail. Large vertical gradients of rain rate at the lowest altitudes, especially for warm rain, provide a second factor that may contribute to varying pre-factors in K_{DP} relationships. Strong downdrafts provide a third mechanism leading to varying pre-factors in polarimetric algorithms. Bias adjustments based on rain gauge and bucket survey observations will likely continue to prove useful for useful for computing rainfall fields used for storm catalogs and PMP estimates.

Rainfall variability for the remnants of Ida (as illustrated, e.g., in Figures 16 and 17) is striking. New methods for quantifying space-time variability of rainfall are needed along the lines envisioned by Le Cam (1961) and Waymire et al. (1984). The goal of these studies was to mesh physical representations of rainfall with statistical models, largely based on point process representations of initiation, motion and structure of storm cells. From a practical standpoint, the absence of a sound statistical model of extreme rainfall in time and space has resulted in the reliance on ad-hoc adjustments for translating point estimates of precipitation frequency to areal assessments (Wright et al., 2020). Lagrangian analyses of rainfall fields from Ida provide a conceptual framework for examining rainfall variability of storms producing extreme rainfall over sub-daily time scales.

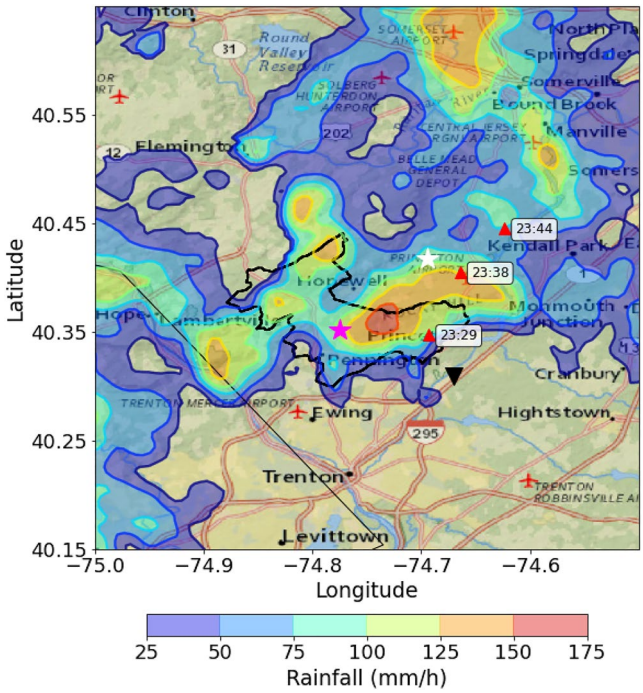

Figure 19. Radar rain rate field (mm hr^{-1}) at 2330 UTC on 1 September with Stony Brook basin boundary; mesocyclone locations at 2329, 2338, and 2344 UTC are denoted by red triangles. Inverted black triangle shows location of the Princeton tornado (EF1) at 2330 UTC. Magenta star marks location of the Hopewell, NJ rain gauge; white star is location of the Skillman rain gauge (see also Figure 7 and Table 1).

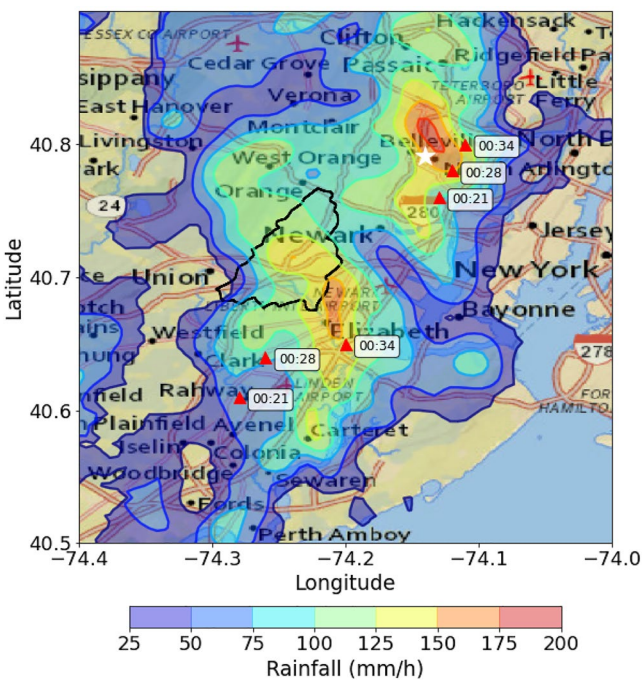

Figure 20. Radar rain rate field at 0038 UTC on 2 September with Elizabeth River basin boundary. Mesocyclone locations at 0021, 0028, and 0034 for two supercells are denoted by red triangles. White star marks location of the North Arlington CoCoRaHS station.

The center of storm circulation is the frame of reference for "physics-based tropical cyclone rainfall models" used for examining the changing climatology of tropical cyclone rainfall in a warming climate (Feldmann et al., 2019; Lu et al., 2018; Xi et al., 2020). The distribution of rainfall relative to the center of circulation of a tropical cyclone changes rapidly as the storm moves over land, especially for transitioning storms. The evolution of extreme rainfall from the remnants of Ida illustrates the difficulties in modeling tropical cyclone rainfall over land in the mid-latitudes.

Quantifying the evolving frequency of short-duration rainfall extremes is a challenge for climate change assessments (Fowler et al., 2021; Prein et al., 2016; Westra et al., 2014). From a practical standpoint, revising the NOAA Precipitation Frequency results (Bonin et al., 2016) is a critical step for addressing flood hazards. For sub-daily time scales, the sparsity of rain gauge data is a major obstacle to development of updated precipitation frequency products. For the eastern Pennsylvania—New Jersey region, only a handfull of long-term rain gauge observations are available for precipitation frequency studies (DeGaetano & Tran, 2021). Radar rainfall data sets provide an important resource for future precipitation frequency studies (Saltikoff et al., 2019).

Ida was a "strange storm" based on the record rainfall totals and flood peaks and based on the prominent role of tropical cyclone supercells as agents of extreme rainfall in the Northeastern US. Smith et al. (2018) refer to flood events for which the ratio of the record flood peak to the 10-year flood magnitude (the Upper Tail Ratio) is large as "strange floods." The strangest flood in the USGS stream gaging record is the June 1903 Heppner flood, which has an Upper Tail Ratio of 200, that is, the June 1903 flood peak was 200 times larger than the sample 10-year flood magnitude. The Heppner Flood, which resulted in more than 250 fatalities, was the product of extreme rainfall from a supercell in a setting dominated by snowmelt floods.

Characterizing the "nature" of the upper tail of rainfall is central to advances in methods used for precipitation frequency analysis and for computing PMP. The extreme nature of rainfall from Ida may derive from the unusual interplay of common heavy rainfall ingredients. Or the rainfall extremes may reflect systematic changes that create Ida-like convective environments more frequently in a warming climate—a challenging scenario for extreme rainfall and flood hazards in the Northeastern US.

7. Summary and Conclusions

In this study, we examine rainfall extremes from the remnants of Hurricane Ida in eastern Pennsylvania and New Jersey. Polarimetric radar analyses provide the grounding for rainfall assessments and for characterization of the storms responsible for rainfall extremes. The principal conclusions of the study are summarized below.

- Rainfall accumulations on 1–2 September 2021 exceeded 1000-year magnitudes, based on NOAA Atlas 14, for time intervals ranging from 1 to 3 hr at numerous locations in an arc from eastern Pennsylvania to New York City. Paired with rainfall extremes were record flood peaks at USGS stream gaging stations. The flood peak in the Elizabeth River—the setting for multiple flood fatalities—is one of the most extreme in the USGS record for the Eastern US (Smith et al., 2018).

- Supercells were the principal agents of extreme rainfall and flooding on 1 September. Long-lived supercells and clusters of supercells contributed to the spatial and temporal pattern of rainfall extremes. The size of extreme rainfall regions from individual supercells was an important factor in dictating rainfall variability for watersheds experiencing record flooding from Ida. Cycles of mesocyclone growth and occlusion likely contributed to the pulsating nature of extreme rainfall in time and the large spatial gradients in rainfall. Future research should more fully address polarimeteric signatures of extreme rainfall in supercells.
- Like other extreme flood events from tropical cyclones in the Northeastern US, Extratropical Transition was a key element of extreme rainfall from Ida. Tropical and extratropical components of storm evolution contributed to extremes of precipitable water, IVT and CAPE. Extremes of atmospheric water balance components for Ida are comparable to those from five tropical cyclones—Diane (1955), Doria (1971), Agnes (1972), Floyd (1999), and Irene (2011)—that dominate the upper tail of flood peak distributions in eastern Pennsylvania and New Jersey. Analyses of reanalysis fields suggest that CAPE values for Diane, Doria, Agnes, Floyd, and Irene were smaller than those from Ida.
- The remnants of Ida not only produced record flood peaks at USGS stream gaging stations, but also anomalously rapid rising limbs of the flood hydrograph, relative to other tropical cyclone floods. Extreme flood response from Ida was closely linked to short-duration rainfall extremes.
- Polarimetric radar fields—in particular, specific differential phase shift, K_{DP}—provide accurate measurements of extreme rainfall at fine temporal and spatial scales for the regions of heaviest rainfall from Ida. Gauge—radar intercomparisons suggest that K_{DP} measurements can play an increasing role in developing rainfall estimates for extreme storms. Future research should more closely examine strengths and limitations of K_{DP}-based rainfall estimates (Kumjian, 2013; A. Ryzhkov et al., 2022). The enhanced low elevation scanning strategy employed for Ida—largely due to the tornado threat—provided 2 min time resolution for rainfall fields. Rapid low elevation scans are especially useful for rainfall estimation in supercells due to their rapid motion and evolution.

Data Availability Statement

WSR-88D Level II polarimetric fields are available from the National Centers for Environmental Information (NCEI) at https://www.ncdc.noaa.gov/nexradinv/. We use the "bulk download" option for accessing Level II fields. Code used for processing Level II polarimetric fields can be obtained from the Py-ART github site (https://arm-doe.github.io/pyart/; see Helmus and Collis (2016)). Code used for computing specific differential phase shift from Level II polarimetric fields can be obtained from the CSU-RadarTools github site (https://github.com/CSU-Radarmet/CSURadarTools). SPORK-SPIN algorithms used for rotational motion can be found at https://github.com/mwilson14/SPORK-SPIN. NEXRAD Stage IV rainfall fields can be obtained from https://rda.ucar.edu/datasets/ds507.5/. GDAS analysis fields can be obtained at https://rda.ucar.edu/datasets/ds083.3/. USGS streamflow and rain gauge data are available at https://waterdata.usgs.gov/usa/nwis. Rain gauge data from the Rutgers New Jersey Weather network can be downloaded at https://www.njweather.org/data. Rain gauge data from the CoCoRaHS network can be downloaded at https://www.cocorahs.org.

Acknowledgments
The authors gratefully acknowledge the helpful comments and suggestions from Dan Chavas (Purdue), Kerry Emanuel (MIT), John England (US Army Corps of Engineers), Jonathan Gourley (NSSL), Erik Nielsen (Texas *A&M*), David Robinson (Rutgers), Alexander Ryzhkov (University of Oklahoma), Russ Schumacher (Colorado State University), Matthew Van Den Broeke (University of Nebraska), Matt Wilson (University of Nebraska) and four anonymous reviewers. Special thanks to Matt Wilson for help in implementing procedures used for mesocyclone detection. This research was supported by the National Science Foundation (EAR-1632048), NOAA CIMES and the Moore Foundation.

References

Allen, R. J., & DeGaetano, A. T. (2005). Considerations for the use of radar-derived precipitation estimates in determining return intervals for extreme areal precipitation amounts. *Journal of Hydrology*, *315*(1–4), 203–219. https://doi.org/10.1016/j.jhydrol.2005.03.028

Atallah, E., & Bosart, L. F. (2003). The extratropical transition and precipitation distribution of Hurricane Floyd (1999). *Monthly Weather Review*, *131*(6), 1063–1081. https://doi.org/10.1175/1520-0493(2003)131<1063:tetapd>2.0.co;2

Atallah, E., Bosart, L. F., & Aiyyer, A. R. (2007). Precipitation distribution associated with landfalling tropical cyclones over the eastern United States. *Monthly Weather Review*, *135*(6), 2185–2206. https://doi.org/10.1175/mwr3382.1

AWA. (2019). *Probable maximum precipitation study for Pennsylvania (Technical report)*. Applied Weather Associates.

Bailey, J. F., Patterson, J. L., & Paulhus, J. L. H. (1975). *Hurricane Agnes rainfall and floods June-July 1972 (U.S. Geological Prof. Paper No. 924)*. USGS.

Berne, A., & Krajewski, W. F. (2013). Radar for hydrology: Unfulfilled promise or unrecognized potential? *Advances in Water Resources*, *51*, 357–366. https://doi.org/10.1016/j.advwatres.2012.05.005

Beven, J. L., Hagen, A., & Berg, R. (2022). *Hurricane Ida (Tropical cyclone report)*. National Hurricane Center.

Bonin, G. M., Martin, D., Lin, B., Parzybok, T., Yetka, M., & Riley, D. (2016). *NOAA Atlas 14: Precipitation frequency Atlas of the United States, volume 2 version 3.0 (Technical Report). Silver spring*. National Weather Service.

Braud, I., Ayral, P.-A., Bouvier, C., Branger, F., Delrieu, G., Le Coz, J., et al. (2014). Multi-scale hydrometeorological observation and modelling for flash flood understanding. *Hydrology and Earth System Sciences*, *18*(9), 3733–3761. https://doi.org/10.5194/hess-18-3733-2014

Bunkers, M. J., Hjelmfelt, M. R., & Smith, P. L. (2006). An observational examination of long-lived supercells. Part I: Characteristics, evolution, and demise. *Weather and Forecasting*, *11*(5), 673–688. https://doi.org/10.1175/waf949.1

Chandrasekar, V., Bringi, V., Balakrishnan, N., & Zrnić, D. (1990). Error structure of multiparameter radar and surface measurements of rainfall. Part III: Specific differential phase. *Journal of Atmospheric and Oceanic Technology*, *7*(5), 621–629. https://doi.org/10.1175/1520-0426(1990)007<0621:esomra>2.0.co;2

Chaney, M. M., Smith, J. A., & Baeck, M. L. (2022). Range dependence of polarimetric radar estimates for extreme flood-producing rainfall in Urban watersheds. *Journal of Hydrometeorology*, *23*(8), 1205–1226. https://doi.org/10.1175/jhm-d-21-0191.1

Cho, J. Y., Kurdzo, J. M., Bennett, B. J., Weber, M. E., Dellicarpini, J. W., Loconto, A., & Frank, H. (2022). Impact of WSR-88D intra-volume low-level scans on severe weather warning performance. *Weather and Forecasting*, *37*(7), 1169–1189. https://doi.org/10.1175/waf-d-21-0152.1

Colle, B. A. (2003). Numerical simulations of the extratropical transition of Floyd (1999): Structural evolution and responsible mechanisms for the heavy rainfall over the Northeast U.S. *Monthly Weather Review*, *131*(12), 2905–2926. https://doi.org/10.1175/1520-0493(2003)131<2905:nsotet>2.0.co;2

Cotton, W. L., & Anthes, R. (1989). *Storm and cloud dynamics*. Academic Press.

Davenport, C. E. (2021). Environmental evolution of long-lived supercell thunderstorms in the great plains. *Weather and Forecasting*, *36*(6), 2187–2209. https://doi.org/10.1175/waf-d-21-0042.1

DeGaetano, A., & Tran, H. (2021). *Changes in hourly and daily extreme rainfall amounts in New Jersey since the publication of NOAA Atlas 14 (Technical report)*. Cornell University.

Derber, J. C., Parrish, D. F., & Lord, S. J. (1991). The new global operational analysis system at the National Meteorological Center. *Weather and Forecasting*, *6*(4), 538–547. https://doi.org/10.1175/1520-0434(1991)006<0538:tngoas>2.0.co;2

DiMego, G. J., & Bosart, L. F. (1982). The transformation of Tropical Storm Agnes into an extratropical cyclone. Part I: The observed fields and vertical motion computations. *Monthly Weather Review*, *110*(5), 385–411. https://doi.org/10.1175/1520-0493(1982)110<0385:ttotsa>2.0.co;2

Dixon, M., & Wiener, G. (1993). TITAN—Thunderstorm identification, tracking, analysis, and nowcasting—A radar-based methodology. *Journal of Atmospheric and Oceanic Technology*, *10*(6), 785–797. https://doi.org/10.1175/1520-0426(1993)010<0785:ttitaa>2.0.co;2

Doswell, C. A., Brooks, H. E., & Maddox, R. A. (1996). Flash flood forecasting: An ingredients-based methodology. *Weather and Forecasting*, *11*(4), 560–581. https://doi.org/10.1175/1520-0434(1996)011<0560:fffaib>2.0.co;2

Edwards, R. (2012). Tropical cyclone tornadoes: A review of knowledge in research and prediction. *Electronic Journal of Severe Storms Meteorology*, *7*(6), 1–61. https://doi.org/10.55599/ejssm.v7i6.42

Edwards, R., Overpeck, S., Woodall, G. R., & Nowotarski, C. J. (2018). Tornadoes in Hurricane Harvey: Documentation and environmental analysis. In *29th conference on severe local storms*.

Feldmann, M., Emanuel, K., Zhu, L., & Lohmann, U. (2019). Estimation of Atlantic tropical cyclone rainfall frequency in the United States. *Journal of Applied Meteorology and Climatology*, *58*(8), 1853–1866. https://doi.org/10.1175/jamc-d-19-0011.1

Fowler, H. J., Ali, H., Allan, R. P., Ban, N., Barbero, R., Berg, P., et al. (2021). Towards advancing scientific knowledge of climate change impacts on short-duration rainfall extremes. *Philosophical Transactions of the Royal Society A*, *379*(2195), 20190542. https://doi.org/10.1098/rsta.2019.0542

Fulton, R., Breidenbach, J. P., Seo, D. J., Miller, D. A., & O'Bannon, T. (1998). The WSR-88D rainfall algorithm. *Weather and Forecasting*, *13*(2), 377–398. https://doi.org/10.1175/1520-0434(1998)013<0377:twra>2.0.co;2

Galarneau, T. J., Bosart, L. F., & Schumacher, R. S. (2010). Predecessor rain events ahead of tropical cyclones. *Monthly Weather Review*, *138*(8), 3272–3297. https://doi.org/10.1175/2010mwr3243.1

Ghebreyesus, D. T., & Sharif, H. O. (2021). Development and assessment of high-resolution radar-based precipitation intensity-duration-curve (IDF) curves for the state of Texas. *Remote Sensing*, *13*(2890), 2890. https://doi.org/10.3390/rs13152890

Giangrande, S. E., & Ryzhkov, A. V. (2008). Estimation of rainfall based on the results of polarimetric echo classification. *Journal of Applied Meteorology and Climatology*, *47*(9), 2445–2462. https://doi.org/10.1175/2008jamc1753.1

Hansen, E. M. (1987). Probable maximum precipitation for design floods in the United States. *Journal of Hydrology*, *96*(1–4), 267–278. https://doi.org/10.1016/0022-1694(87)90158-2

Hart, R. E., & Evans, J. L. (2001). A climatology of the extratropical transition of Atlantic tropical cyclones. *Journal of Climate*, *14*(4), 546–564. https://doi.org/10.1175/1520-0442(2001)014<0546:acotet>2.0.co;2

Helmus, J. J., & Collis, S. M. (2016). The Python ARM radar Toolkit (Py-ART), a library for working with weather radar data in the Python programming language. *Journal of Open Research Software*, *4*(1), e25. https://doi.org/10.5334/jors.119

Hirschboeck, K. K. (1987). Hydroclimatically defined mixed distributions in partial duration flood series. In V. P. Singh (Ed.), *Hydrologic frequency modelling* (pp. 199–212). D. Reidel Publishing Company.

Imhoff, R., Brauer, C., van Heeringen, K.-J., Leijnse, H., Overeem, A., Weerts, A., & Uijlenhoet, R. (2021). A climatological benchmark for operational radar rainfall bias reduction. *Hydrology and Earth System Sciences*, *25*(7), 4061–4080. https://doi.org/10.5194/hess-25-4061-2021

Jung, C., & Lackmann, G. M. (2019). Extratropical transition of Hurricane Irene (2011) in a changing climate. *Journal of Climate*, *32*(15), 4847–4871. https://doi.org/10.1175/jcli-d-18-0558.1

Kingfield, D. M., & French, M. M. (2022). The influence of WSR-88D intra-volume scanning strategies on thunderstorm observations and warnings in the dual-polarization radar era: 2011–2020. *Weather and Forecasting*, *37*(2), 283–301. https://doi.org/10.1175/waf-d-21-0127.1

Knupp, K. R., Murphy, T. A., Coleman, T. A., Wade, R. A., Mullins, S. A., Schultz, C. J., et al. (2014). Meteorological overview of the devastating 27 April 2011 tornado outbreak. *Bulletin of the American Meteorological Society*, *95*(7), 1041–1062. https://doi.org/10.1175/bams-d-11-00229.1

Kumjian, M. R. (2011). Precipitation properties of supercell hook echoes. *Electronic Journal Severe Storms Meteorology*, *6*(5), 1–21. https://doi.org/10.55599/ejssm.v6i5.32

Kumjian, M. R. (2013). Principles and applications of dual-polarization radar. *Journal of Operational Meteorology*, *1*(19–21), 226–274. https://doi.org/10.15191/nwajom.2013.0119

Kumjian, M. R., & Ryzhkov, A. V. (2008). Polarimetric signatures in supercell thunderstorms. *Journal of Applied Meteorology and Climatology*, *47*(7), 1940–1961. https://doi.org/10.1175/2007jamc1874.1

Kumjian, M. R., Ryzhkov, A. V., Melnikov, V. M., & Schuur, T. J. (2010). Rapid-scan super-resolution observations of a cyclic supercell with a dual-polarization WSR-88D. *Monthly Weather Review*, *138*(10), 3762–3786. https://doi.org/10.1175/2010mwr3322.1

Kunkel, K. E., Karl, T. R., Eastering, D. R., Redmond, K., Young, J., Yin, X., & Hennon, P. (2013). Probable maximum precipitaton and climate change. *Geophysical Research Letters*, *40*(7), 1402–1408. https://doi.org/10.1002/grl.50334

Kuster, C. M., Bowers, B. R., Carlin, J. T., Schuur, T. J., Brogden, J. W., Toomey, R., & Dean, A. (2021). Using K_{DP} cores as a downburst precursor signature. *Weather and Forecasting*, *36*(4), 1183–1198. https://doi.org/10.1175/waf-d-21-0005.1

Lang, T. J., Ahijevych, D. A., Nesbitt, S. W., Carbone, R. E., Rutledge, S. A., & Cifelli, R. (2007). Radar-observed characteristics of precipitating systems during NAME 2004. *Journal of Climate*, *20*(9), 1713–1733. https://doi.org/10.1175/jcli4082.1

Le Cam, L. M. (1961). A stochastic description of precipitation. In J. Neyman (Ed.), *Proceedings of the fourth Berkeley symposium on mathematical statistics and probability* (pp. 165–186).
Lengfeld, K., Kirstetter, P.-E., Fowler, H. J., Yu, J., Becker, A., Flamig, Z., & Gourley, J. (2020). Use of radar data for characterizing extreme precipitation at fine scales and short durations. *Environmental Research Letters*, *15*(8), 085003. https://doi.org/10.1088/1748-9326/ab98b4
Lin, Y., & Mitchell, K. E. (2005). The NCEP stage II/IV hourly precipitation analyses: Development and applications. In *AMS 19th conference on hydrology*. American Meteorological Society.
Liu, M., & Smith, J. A. (2016). Extreme rainfall from landfalling tropical cyclones in the eastern United States: Hurricane Irene (2011). *Journal of Hydrometeorology*, *17*(11), 2883–2904. https://doi.org/10.1175/jhm-d-16-0072.1
Liu, M., Vecchi, G. A., Smith, J. A., & Murakami, H. (2017). The present-day simulation and twenty-first-century projection of the climatology of extratropical transition in the North Atlantic. *Journal of Climate*, *30*(8), 2739–2756. https://doi.org/10.1175/jcli-d-16-0352.1
Liu, M., Yang, L., Smith, J., & Vecchi, G. (2020). Response of extreme rainfall for landfalling tropical cyclones undergoing extratropical transition to projected climate change: Hurricane Irene (2011). *Earth's Future*, *8*(3), e2019EF001360. https://doi.org/10.1029/2019ef001360
Loeffler, S. D., Kumjian, M. R., Jurewicz, M., & French, M. M. (2020). Differentiating between tornadic and nontornadic supercells using polarimetric radar signatures of hydrometeor size sorting. *Geophysical Research Letters*, *47*(12), e2020GL088242. https://doi.org/10.1029/2020gl088242
Lu, P., Lin, N., Emanuel, K., Chavas, D., & Smith, J. (2018). Assessing hurricane rainfall mechanisms using a physics-based model: Hurricanes Isabel (2003) and Irene (2011). *Journal of the Atmospheric Sciences*, *75*(7), 2337–2358. https://doi.org/10.1175/jas-d-17-0264.1
Markowski, P., & Richardson, Y. (2011). *Mesoscale meteorology in midlatitudes* (Vol. 2). John Wiley & Sons.
Marra, F., Morin, E., Peleg, N., Mei, Y., & Anagnostou, E. N. (2017). Intensity–duration–frequency curves from remote sensing rainfall estimates: Comparing satellite and weather radar over the eastern Mediterranean. *Hydrology and Earth System Sciences*, *21*(5), 2389–2404. https://doi.org/10.5194/hess-21-2389-2017
Marra, F., Nikolopoulos, E. I., Anagnostou, E. N., & Morin, E. (2018). Metastatistical extreme value analysis of hourly rainfall from short records: Estimation of high quantiles and impact of measurement errors. *Advances in Water Resources*, *117*, 27–39. https://doi.org/10.1016/j.advwatres.2018.05.001
Matyas, C. J. (2017). Comparing the spatial patterns of rainfall and atmospheric moisture among tropical cyclones having a track similar to Hurricane Irene (2011). *Atmosphere*, *8*(9), 165. https://doi.org/10.3390/atmos8090165
McCaul, E. W. (1991). Buoyancy and shear characteristics of hurricane-tornado environments. *Monthly Weather Review*, *119*(8), 1954–1978. https://doi.org/10.1175/1520-0493(1991)119<1954:bascoh>2.0.co;2
McGraw, D., Nikolopoulos, E. I., Marra, F., & Anagnostou, E. N. (2019). Precipitation frequency analyses based on radar estimates: An evaluation over the contiguous United States. *Journal of Hydrology*, *573*, 299–310. https://doi.org/10.1016/j.jhydrol.2019.03.032
Merz, R., & Blöschl, G. (2003). A process typology of regional floods. *Water Resources Research*, *39*(12), 1340. https://doi.org/10.1029/2002WR001952
Miniussi, A., Marani, M., & Villarini, G. (2020). Metastatistical extreme value distribution applied to floods across the continental United States. *Advances in Water Resources*, *136*, 103498. https://doi.org/10.1016/j.advwatres.2019.103498
Molter, E. M., Collins, W. D., & Risser, M. D. (2021). Quantitative precipitation estimation of extremes in conus with radar data. *Geophysical Research Letters*, *48*(16), e2021GL094697. https://doi.org/10.1029/2021gl094697
Morgan, A. E. (1917). *The Miami valley flood-protection work: Fixing maximum flood limits* (pp. 2–7). Engineering News.
Morin, E., Goodrich, D. C., Maddox, R. A., Gao, X. G., Gupta, H. V., & Sorooshian, S. (2006). Spatial patterns in thunderstorm rainfall events and their coupling with watershed hydrological response. *Advances in Water Resources*, *29*(6), 843–860. https://doi.org/10.1016/j.advwatres.2005.07.014
Nielsen, E. R., & Schumacher, R. S. (2018). Dynamical insights into extreme short-term precipitation associated with supercells and mesovortices. *Journal of the Atmospheric Sciences*, *75*(9), 2983–3009. https://doi.org/10.1175/JAS-D-17-0385.1
Nielsen, E. R., & Schumacher, R. S. (2020a). Dynamical mechanisms supporting extreme rainfall accumulations in the Houston "Tax Day" Flood. *Monthly Weather Review*, *148*(1), 83–109. https://doi.org/10.1175/MWR-D-19-0206
Nielsen, E. R., & Schumacher, R. S. (2020b). Observations of extreme short-term precipitation associated with supercells and mesovortices. *Monthly Weather Review*, *148*(1), 159–182. https://doi.org/10.1175/mwr-d-19-0146.1
Nowotarski, C. J., Spotts, J., Edwards, R., Overpeck, S., & Woodall, G. R. (2021). Tornadoes in Hurricane Harvey. *Weather and Forecasting*, *36*(5), 1589–1609. https://doi.org/10.1175/waf-d-20-0196.1
NRC. (1994). *Estimating bounds on extreme precipitation events: A brief assessment (Technical Report)*. National Research Council, National Academy Press.
Overeem, A., Buishand, A., & Holleman, I. (2009). Extreme rainfall analysis and estimation of depth-duration-frequency curves using weather radar. *Water Resources Research*, *45*, W10424. https://doi.org/10.1029/2009WR007869
Prein, A. F., Rasmussen, R. M., Ikeda, K., Liu, C., Clark, M. P., & Holland, G. J. (2016). The future intensification of hourly precipitation extremes. *Nature Climate Change*, *7*(1), 48–52. https://doi.org/10.1038/NCLIMATE3168
Reimel, K. J., & Kumjian, M. (2021). Evaluation of K DP estimation algorithm performance in rain using a known-truth framework. *Journal of Atmospheric and Oceanic Technology*, *38*(3), 587–605. https://doi.org/10.1175/jtech-d-20-0060.1
Romine, R. S., Burgess, D. W., & Wilhelmson, R. B. (2008). A dual-polarization-radar-based assessment of the 8 May 2003 Oklahoma city area tornadic supercell. *Monthly Weather Review*, *136*, 2849–2870. https://doi.org/10.1175/2008mwr2330.1
Ryzhkov, A., Zhang, P., Bukovčić, P., Zhang, J., & Cocks, S. (2022). Polarimetric radar quantitative precipitation estimation. *Remote Sensing*, *14*(7), 1695. https://doi.org/10.3390/rs14071695
Ryzhkov, A. V., Schuur, T. J., Burgess, D. W., Heinselman, P. L., Giangrande, S. E., & Zrnić, D. S. (2005). The joint polarization experiment: Polarimetric rainfall measurements and hydrometeor classification. *Bulletin of the American Meteorological Society*, *86*(6), 809–824. https://doi.org/10.1175/bams-86-6-809
Saharia, M., Kirstetter, P.-E., Vergara, H., Gourley, J. J., Hong, Y., & Giroud, M. (2017). Mapping flash flood severity in the United States. *Journal of Hydrometeorology*, *18*(2), 397–411. https://doi.org/10.1175/jhm-d-16-0082.1
Saltikoff, E., Friedrich, K., Soderholm, J., Lengfeld, K., Nelson, B., Becker, A., et al. (2019). An overview of using weather radar for climatological studies: Successes, challenges, and potential. *Bulletin of the American Meteorological Society*, *100*(9), 1739–1752. https://doi.org/10.1175/bams-d-18-0166.1
Schleiss, M., Olsson, J., Berg, P., Niemi, T., Kokkonen, T., Thorndahl, S., et al. (2020). The accuracy of weather radar in heavy rain: A comparative study for Denmark, The Netherlands, Finland and Sweden. *Hydrology and Earth System Sciences*, *24*(6), 3157–3188. https://doi.org/10.5194/hess-24-3157-2020

Schoner, R. W., & Molansky, S. (1956). *Rainfall associated with hurricanes and other tropical disturbances. (Technical Report)*. U. S. National Hurricane Research Project.
Schreiner, L. C., & Riedel, J. T. (1978). *Probable maximum precipitation estimates, United States east of the 105th meridian. (Hydrometeorological Report No. 51)*. NOAA National Weather Service.
Schultz, L. A., & Cecil, D. J. (2009). Tropical cyclone tornadoes, 1950–2007. *Monthly Weather Review*, *137*(10), 3471–3484. https://doi.org/10.1175/2009mwr2896.1
Seo, D. J., Breidenbach, J. P., & Johnson, E. R. (1999). Real-time estimation of mean field bias in radar rainfall data. *Journal of Hydrology*, *223*(3–4), 131–147. https://doi.org/10.1016/s0022-1694(99)00106-7
Seo, D.-J., Siddique, R., Zhang, Y., & Kim, D. (2014). Improving real-time estimation of heavy-to-extreme precipitation using rain gauge data via conditional bias-penalized optimal estimation. *Journal of Hydrology*, *519*, 1824–1835. https://doi.org/10.1016/j.jhydrol.2014.09.055
Smith, J. A., Back, M. L., Yang, L., Signell, J., Morin, E., & Goodrich, D. C. (2019). The paroxysmal precipitation of the desert: Flash floods in the southwestern US. *Water Resources Research*, *55*(12), 10218–10247. https://doi.org/10.1029/2019WR025480
Smith, J. A., Baeck, M. L., Zhang, Y., & Doswell, C. A., III. (2001). Extreme rainfall and flooding from supercell thunderstorms. *Journal of Hydrometeorology*, *2*(5), 469–489. https://doi.org/10.1175/1525-7541(2001)002<0469:eraffs>2.0.co;2
Smith, J. A., Baeck, M. L., Villarini, G., Welty, C., Miller, A. J., & Krajewski, W. F. (2012). Analyses of a long-term high-resolution radar rainfall data set for the Baltimore metropolitan region. *Water Resources Research*, *48*(4), W04504. https://doi.org/10.1029/2011wr010641
Smith, J. A., Cox, A. A., Baeck, M. L., Yang, L., & Bates, P. (2018). Strange floods: The upper tail of flood peaks in the US. *Water Resources Research*, *54*(9), 6510–6542. https://doi.org/10.1029/2018wr022539
Smith, J. A., & Krajewski, W. F. (1991). Estimation of the mean field bias of radar rainfall estimates. *Journal of Applied Meteorology*, *30*(4), 397–412. https://doi.org/10.1175/1520-0450(1991)030<0397:eotmfb>2.0.co;2
Smith, J. A., Villarini, G., & Baeck, M. L. (2011). Mixture distributions and the climatology of extreme rainfall and flooding in the eastern US. *Journal of Hydrometeorology*, *12*(2), 294–309. https://doi.org/10.1175/2010jhm1242.1
Snyder, J. C., Ryzhkov, A. V., Kumjian, M. R., Khain, A. P., & Picca, J. (2015). A ZDR column detection algorithm to examine convective storm updrafts. *Weather and Forecasting*, *30*(6), 1819–1844. https://doi.org/10.1175/waf-d-15-0068.1
Su, Y., & Smith, J. A. (2021). An atmospheric water balance perspective on extreme rainfall potential for the contiguous US. *Water Resources Research*, *57*(4), e2020WR028387. https://doi.org/10.1029/2020wr028387
Trapp, R. J., Marion, G. R., & Nesbitt, S. W. (2017). The regulation of tornado intensity by updraft width. *Journal of the Atmospheric Sciences*, *74*(12), 4199–4211. https://doi.org/10.1175/jas-d-16-0331.1
United States Weather Bureau. (1955). Preliminary report of Hurricane Diane and floods in northeast (Technical report). Author. Retrieved from http://docs.lib.noaa.gov/rescue/hurricanes/QC9452D53H81955a.pdf
U.S. Army Corps of Engineers. (1973). Storm rainfall in the United States, 1945–1973 (Technical report). Author.
Van Den Broeke, M. (2021). Polarimetric radar characteristics of tornadogenesis failure in supercell thunderstorms. *Atmosphere*, *12*(5), 581. https://doi.org/10.3390/atmos12050581
Van Den Broeke, M. S. (2015). Polarimetric tornadic debris signature variability and debris fallout signatures. *Journal of Applied Meteorology and Climatology*, *54*(12), 2389–2405. https://doi.org/10.1175/jamc-d-15-0077.1
Van Den Broeke, M. S. (2020). A preliminary polarimetric radar comparison of pretornadic and nontornadic supercell storms. *Monthly Weather Review*, *148*(4), 1567–1584. https://doi.org/10.1175/mwr-d-19-0296.1
Villarini, G. (2016). On the seasonality of flooding across the continental United States. *Advances in Water Resources*, *87*, 80–91. https://doi.org/10.1016/j.advwatres.2015.11.009
Villarini, G., & Smith, J. A. (2010). Flood peak distributions for the eastern United States. *Water Resources Research*, *46*, W06504. https://doi.org/10.1029/2009WR008395
Villarini, G., Smith, J. A., Baeck, M. L., Marchock, T., & Vecchi, G. A. (2011). Characterization of rainfall distribution and flooding associated with U.S. landfalling tropical cyclones: Analyses of Hurricanes Frances, Ivan, and Jeanne (2004). *Journal of Geophysical Research*, *116*(D23), D23116. https://doi.org/10.1029/2011jd016175
Wang, Y., & Chandrasekar, V. (2009). Algorithm for estimation of the specific differential phase. *Journal of Atmospheric and Oceanic Technology*, *26*(12), 2565–2578. https://doi.org/10.1175/2009jtecha1358.1
Waymire, E., Gupta, V. K., & Rodriguez-Iturbe, I. (1984). Spectral theory of rainfall intensity at the meso-β scale. *Water Resources Research*, *20*(10), 1453–1465. https://doi.org/10.1029/wr020i010p01453
Westra, S., Fowler, H. J., Evans, J. P., Alexander, L. V., Berg, P., Johnson, F., et al. (2014). Future changes to the intensity and frequency of short-duration rainfall. *Reviews of Geophysics*, *52*(3), 522–555. https://doi.org/10.1002/2014rg000464
Wilson, M. B., Humrich, N. R., & Van Den Broeke, M. S. (2020). The supercell polarimetric observation research kit (SPORK): An automated, python-based algorithm for examining supercell dual-pol signatures. *100th American meteorological society annual meeting*.
Wilson, M. B., & Van Den Broeke, M. S. (2021). An automated Python algorithm to quantify ZDR arc and KDP-ZDR separation signatures in supercells. *Journal of Atmospheric and Oceanic Technology*, *38*(2), 371–386. https://doi.org/10.1175/jtech-d-20-0056.1
World Meteorological Organization. (2009). Manual on estimation of probable maximum precipitation (Technical report No. WMO No. 1045).
Wright, D. B., Smith, J. A., & Baeck, M. L. (2014). Flood frequency analysis using radar rainfall fields and stochastic storm transposition. *Water Resources Research*, *50*(2), 1592–1615. https://doi.org/10.1002/2013wr014224
Wright, D. B., Smith, J. A., Villarini, G., & Baeck, M. L. (2013). Estimating the frequency of extreme rainfall using weather radar and stochastic storm transposition. *Journal of Hydrology*, *488*, 150–165. https://doi.org/10.1016/j.jhydrol.2013.03.003
Wright, D. B., Yu, G., & England, J. F., Jr. (2020). Six decades of rainfall and flood frequency analysis using stochastic storm transposition: Review, progress, and prospects. *Journal of Hydrology*, *585*, 124816. https://doi.org/10.1016/j.jhydrol.2020.124816
Xi, D., Lin, N., & Smith, J. (2020). Evaluation of a physics-based tropical cyclone rainfall model for risk assessment. *Journal of Hydrometeorology*, *21*(9), 2197–2218. https://doi.org/10.1175/jhm-d-20-0035.1
Zhang, J., Howard, K., Langston, C., Kaney, B., Qi, Y., Tang, L., et al. (2016). Multi-Radar Multi-Sensor (MRMS) quantitative precipitation estimation: Initial operating capabilities. *Bulletin of the American Meteorological Society*, *97*(4), 621–638. https://doi.org/10.1175/bams-d-14-00174.1
Zhou, Z., Smith, J. A., Wright, D. B., Baeck, M. L., Yang, L., & Liu, S. (2019). Storm catalog-based analysis of rainfall heterogeneity and frequency in a complex terrain. *Water Resources Research*, *55*(3), 1871–1889. https://doi.org/10.1029/2018wr023567
Zipser, E. J., & Liu, C. (2022). Extreme convection vs. Extreme rainfall: A global view. *Current Climate Change Reports*, *7*(4), 1–10. https://doi.org/10.1007/s40641-021-00176-0
Zorzetto, E., Botter, G., & Marani, M. (2016). On the emergence of rainfall extremes from ordinary events. *Geophysical Research Letters*, *43*(15), 8076–8082. https://doi.org/10.1002/2016gl069445